Non-linear Extreme Ultraviolet and X-ray Optics and Spectroscopy

Majed Chergui, Martin Beye, Shaul Mukamel, Cristian Svetina & Claudio Masciovecchio

Non-linear Extreme Ultraviolet and X-ray Optics and Spectroscopy

M. Chergui[1], M. Beye[2], S. Mukamel[3], C. Svetina[4], and C. Masciovecchio[5*]

[1] *Lausanne Centre for Ultrafast Science, ISIC, Ecole Polytechnique Fédérale de Lausanne, 1015 Lausanne, Switzerland*

[2] *Deutsches Elektronen-Synchrotron DESY, Notkestr. 85, 22607 Hamburg, Germany*

[3] *Department of Chemistry and Physics & Astronomy, University of California, Irvine, California 92697-2025, United States*

[4] *Madrid Institute for Advanced Studies, IMDEA Nanociencia, Calle Faraday 9, Ciudad Universitaria de Cantoblanco, Madrid, 28049, Spain.*

[5] *Elettra Sincrotrone Trieste S.C.p.A., 34149 Basovizza, Trieste, Italy*

Abstract:

Novel sources of Extreme Ultraviolet (EUV) to hard X-ray photons, such as High-Harmonic Generation (HHG) table-top systems and X-ray Free Electron lasers (XFEL) is providing the scientific community with short-wavelength (sub-200 nm), intense, coherent, tuneable and ultrashort pulses. These specifications enable non-linear optical and spectroscopic methods in the short wavelength regime, akin to what occurred with Terahertz (THz) to Ultraviolet (UV) non-linear optics and spectroscopy over the past sixty years. The wavelength range of core-transitions provides element-specificity, orbital-selectivity, structural resolution down to the sub-nanometer scale and, for some of the methods, high momentum transfers across typical Brillouin zones. In addition, polarisation control and sub-femtosecond temporal resolution open up new frontiers in Science. In this Roadmap article, we first review the emergence of this nascent field over the past ten years or so, including methods such as sum/difference frequency generation and second harmonic generation, 2-photon absorption, stimulated EUV/X-ray emission/Raman and transient grating spectroscopy. We then discuss the unique opportunities offered by these methods and the novel perspectives they provide for probing elementary dynamical events in a wide variety of systems.

* Corresponding authors: majed.chergui@epfl.ch; martin.beye@desy.de; smukamel@uci.edu; cristian.svetina@imdea.org; claudio.masciovecchio@elettra.eu

I. Introduction:

The advent of the laser in the early 1960s represented a revolution in science and technology that is affecting our lives to this day. One of the most salient developments of this revolution has been the birth of non-linear (NL) optics enabled by the high intensity and coherent laser beams. Indeed, the first observation of two-photon absorption (TPA) by Kaiser and Garrett[1] and second harmonic generation (SHG) by Franken et al[2] in 1961, initiated the field, culminating in its recognition by the Physics Nobel Prize awarded to N. Bloembergen in 1981.[3] Optical-domain (ultraviolet, visible, infrared, terahertz) NL methods constituted a major advance in experimental and theoretical physics, in materials science, in chemistry and in biology. NL optics have played a key role in the expansion of laser technology into fundamental sciences and applications, leading to the birth of photonics and optoelectronics. Indeed, a very wide range of methods have been developed, such as multiphoton absorption that enables excitation of dipole-forbidden transitions and widen the spectroscopic analysis of systems. Processes such as SHG and sum/difference frequency generation (SFG/DFG, see figure 1 top) are due to the second-order susceptibility ($\chi^{(2)}$), and are routinely used in laser laboratories, in particular on non-centrosymmetric samples, e.g., surfaces, interfaces and chiral systems, to provide valuable static and dynamical structural information. They allow generating electric fields at wavelengths different from those of the incoming laser pulses and as such, are very much used for fundamental studies. In systems without inversion symmetry, second-order processes do not occur and in this case, the third-order susceptibility ($\chi^{(3)}$) has to be considered as the lowest order nonlinearity. A notable example of third-order processes is third-harmonic generation (THG) of a laser beam interacting with a crystal, which leads to a tripling of the incoming beam frequency (see Figure 1, bottom).[4] These four-wave mixing techniques further enhance the above capabilities and allow, e.g. via transient grating spectroscopy, to probe transport phenomena (heat, charge, magnetism, etc.) in materials and solutions.

NL methods have been key to generate multicolour pulses for further use in fundamental studies. They are also the basis for introduction of new imaging methods, e.g. based on Coherent Anti-Stokes Raman Scattering (CARS) or stimulated emission depletion (STED) microscopy, that are finding widespread applications, especially in medicine. They have also enabled a number of new developments ranging from metrology to laser machining and from optical communication to optical computers to mention a few.[5]

Pulsed lasers pushed NL methods to the next level because they enable higher and higher peak powers for NL phenomena due to the increasing energy per pulse as well as shorter pulse durations. As a consequence, NL methods have been key to fundamental time-resolved studies, first with picosecond time resolution at the end of the 1960s,[6,7] then with femtosecond (fs) resolution at the end of the 1970s,[8] bringing about another revolution as it became possible to access the time scale of nuclear motion within molecules, materials and proteins that are activated by an initial (pump) pulse. These developments were recognized with the Chemistry Nobel Prize to A. Zewail in 1999.[9] The span and breadth of NL laser methods in both fundamental research and in applications is beyond the scope of this article

and we refer the reader to the many excellent books and review articles that are regularly published in this field. Our purpose here is to examine the recent developments that have led to NL methods being extended to shorter wavelengths that enter the region of core-transitions, i.e. the extreme ultraviolet (EUV) to the hard X-ray range. Definitely, in addition to providing element-selectivity both in the probing and in the excitation, the short wavelengths imply a structural-sensitivity and a change of regime in the definition of symmetry, as now the excitations are localised on atoms rather than on molecules or bands in a solid. At such short wavelengths, matter does appear much more structured than in the macroscopic limit seen by wavelengths that are much longer than atomic distances.

The advent of extreme ultraviolet (EUV), soft and hard X-ray Free Electron Lasers (XFELs) over the past 10-15 years,[10–14] as well as the development of table-top EUV light sources based on high-order harmonic generation (HHG)[15–21] are heralding a new revolution in Science. The several orders of magnitude increase in photon flux per pulse (for XFELs, typically a factor of 10^6) compared to conventional pulsed X-ray sources such as synchrotrons, along with the fs to attosecond (As) pulse duration commonly reached by HHG sources, and nowadays also at XFELs, make these sources game changers for time-resolved X-ray spectroscopic and scattering methods.[22–25] In addition to pushing the limits of these linear pump-probe methods, the high fluxes and peak powers of XFELs and HHG sources are enabling the NL revolution in EUV/X-ray science. This field is nascent, but the past ten to fifteen years have already brought a handful of results, which promises a development akin to what happened following the birth of the laser in the early 1960s.

There has already been a number of reviews that have partly dwelt with these developments, either using HHG sources or XFELs.[25–27] However, in this Roadmap article, we survey the capabilities offered by these light sources and the NL methods they enable. We focus on experiments, at photon energies >50 eV (<25 nm) and the current XFEL upper limit of 20 keV, that have so far been carried out on atomic and molecular systems, on chemical systems and on solid materials. We then elaborate on the perspectives, guided by technological and theoretical developments, that are enabled by these novel methodologies. As most of the EUV/X-ray results have been obtained at XFELs due to their high photon fluxes, this article mostly reports work carried out on such facilities. However, important results have also been demonstrated on table-top HHG sources which, in addition to being important milestones, are also promising in view of transferring the EUV/X-ray NL methods from large scale facilities to the university or industrial laboratories.

II. Instrumentation and Methods

Excellent reviews[28–33] already provide a detailed description of the various HHG and XFEL sources of ultrashort EUV/X-ray pulses. In addition, strident progress is continuously being done in enhancing their capabilities. This is the reasons why here, we will only briefly recall the general characteristics of these sources of relevance for EUV/X-ray NL methods.

II.1 X-ray Free electron lasers (XFELs)

X-ray Free Electron Lasers (XFELs) facilities consist of a linear electron accelerator followed by a series of undulators i.e. periodic magnetic devices. The electron bunches are accelerated to relativistic speeds and, once in the undulator, they undergo a periodically alternating transverse acceleration releasing photons through the synchrotron process.[32,33] In FELs the emitted electromagnetic field becomes sufficiently strong and its interaction with the transverse electron current causes some electrons to gain and others to lose energy to the radiation field via the ponderomotive force. This energy modulation evolves into electron density modulations with a period of one wavelength, such that the electron density in a bunch becomes distributed periodically in micro-bunches. The electrons emit radiation in phase, and the emitted photons add up together coherently. The FEL radiation intensity increases, causing additional electron microbunching, which continues to radiate in phase until the electrons are completely micro-bunched and a saturation is reached at which the radiation power is orders of magnitude higher than that of the incoherent undulator radiation of a synchrotron. This is known as the Self Amplified Spontaneous Emission (SASE) process.[34] SASE pulses are characterised by a time/energy structure that is the envelope of a series of sub-pulses with random intensity, time duration, spectral bandwidth and phase. XFEL SASE pulses have tens of femtosecond duration and sub-Å wavelengths but limited temporal coherence, as the initial amplification arises from the electron-beam shot noise.

The first short wavelength FEL to be available to users was FLASH at DESY (Hamburg, Germany) in 2005, which provided extreme ultraviolet (EUV) pulses up to 90.5 eV (13.7 nm) and harmonics reaching the water window (between 280 and 530 eV).[10] The first hard X-ray FEL, the Linac Coherent Light Source (LCLS), was launched in 2009 in Stanford,[12] soon followed by the EUV-FEL FERMI in Italy (Trieste)[35] and the hard XFEL SACLA in Hyogo (Japan).[13] In 2017, three additional hard and soft XFELs went into operation: SwissFEL (Paul Scherrer Institut-PSI. Villigen, Switzerland),[14,36] European XFEL (EuXFEL, Hamburg, Germany)[37,38] and the Pohang Accelerator lab (PAL, Pohang, South Korea),[39] which all operate on the SASE mode.[29]

Amplification of coherent emission relies on the High Gain Harmonic Generation (HGHG) process, which is obtained by seeding the electron bunch with an external laser pulse that imposes an energy modulation on the electron beam. The energy modulation is converted into a density modulation, microbunching, whose spectral content includes higher harmonics of the seed laser.[40] This scheme allows full control of the FEL photon output by acting on the seed laser. Another notable advantage is the preservation of the temporal-coherence of the seed in the emitted FEL radiation, which ensures pulses with longitudinal coherence. The latter is of paramount importance for NL spectroscopies, which require both phase and wavelength manipulation within a given pulse. FERMI (Trieste) is the first machine based on the external seeding scheme. The optical pulse harmonic up-shifting allows reaching output energies >400 eV in the first harmonic, using a cascade scheme or the ECHO-enabled harmonic generation (EEHG) principle[41–43] and pulses of 10's fs. A similar implementation is currently being realised at FLASH, making use of the higher number of pulses per second enabled by the superconducting accelerator.[44] The soft X-ray ATHOS beamline of swissFEL has also

implemented the seeding scheme, with the goal of reaching even higher energies using EEHG. Furthermore, it will deliver pulses with durations of tens to hundreds of As's. We will mention additional upcoming developments in the Outlook section.

II.2 High-Harmonic-Generation (HHG) sources:

HHG sources appeared at the end of the 1980s and have since evolved into the main sources of As-pulses.[45,46] HHG uses an atomic (or even molecular) gas as medium, which under strong field ionization (SFI) launches free electrons that are accelerated under the influence of the oscillatory laser electric field. Upon re-collision with their parent ion, EUV photons are generated by electron–ion recombination.[47] Given that the initial ionization occurs during a short time interval around a maximum of the laser electric field, the duration of the generated EUV pulse is a small fraction that of the driving optical laser pulse, i.e. it lies in the As-domain. The EUV radiation is generated in the form of a comb of harmonics of the energy of the driving laser ($E=hc/\lambda$), whose cut-off energy scales with λ^2. Hence HHG with longer wavelength laser drivers provides a route to table-top sources of high-energy coherent X-ray pulses.[48–50] Indeed, much effort is being devoted at pushing the spectral range of the HHG sources to higher and higher energies reaching the N and O K-edges and even beyond,[51,52] as well as increasing the output pulse energy.[53] Furthermore, the increased repetition rate of HHG sources allows experiments with higher signal-to-noise ratios.[54,55] Although having relatively lower photon fluxes per pulse than XFELs, the table-top nature of HHG sources and their generally higher repetition rates offer more flexibility than XFELs in the planning and performing of experiments. Furthermore, properties of the emitted HHG radiation such as central frequency, cut-off energy, pulse duration, polarisation, etc., can directly be tailored by acting on the driving laser. The most notable feature of HHG sources remains however, the generation of As-pulses. In addition, advanced schemes based on the synthesis of fields in the IR have been proposed for the optimization of the As-pulse generation.[56] This not only breaks into the temporal resolution of the fundamental time scale of electron motion, but it also provides a broad spectral bandwidth for spectroscopy[24,57] as well as high peak powers, which can drive NL processes despite the generally low energy per pulse. Efforts are also undertaken aimed at performing HHG in solids[58] and liquids,[59,60] however these dense media lead to lower cut-off energies than gas phase media.

Much of the early work focused on the generation process in gases, liquids and solids and on attosecond science per se,[15,17,18,47,58,61–68] but thereafter, studies have evolved towards applications such as ultrafast X-ray absorption spectroscopy,[24,25,50,57,57,69,70] photoelectron spectroscopy in gases,[30,71–73] liquids[69,74–77] and solids,[78,79] and non-linear processes such as TG spectroscopy,[80–84] multiphoton ionization,[85,86] pulse compression by 4-wave mixing,[87] and SHG.[88] Below, we discuss some of these achievements.

II.3 Different non-linear schemes enabled by the new sources:

Under high intensity laser radiation, the macroscopic polarisation of matter $\vec{P}$, which is responsible for optical signals, can be expanded in powers of the external electric field amplitude (E):[4,89,90]

$$\vec{P} = \chi^{(1)}\vec{E} + \chi^{(2)}\vec{E}\vec{E} + \chi^{(3)}\vec{E}\vec{E}\vec{E} + \cdots \equiv \vec{P}^{(1)} + \vec{P}^{(2)} + \vec{P}^{(3)} + \cdots, \quad (1)$$

where $\chi^{(N)}$ is a tensor of rank (N+1), usually referred to as N^{th}-order susceptibility, while $\vec{P}^{(N)}$ is the polarisation to N^{th}-order in $\vec{E}$. The value of $\chi^{(N)}$ decreases with increasing N ensuring that the power series converges to a finite $\vec{P}$. Figure 1 sketches the main NL methods due to $\chi^{(2)}$ and $\chi^{(3)}$. The number of independent non-zero elements of $\chi^{(N)}$ is reduced when the material symmetry is taken into account;[4] e.g. all 27 elements of $\chi^{(2)}$ vanish in isotropic materials. $\chi^{(2)}$ is at the origin of 2^{nd}-order phenomena such as sum- (SFG) and difference-frequency generation (DFG) or SHG, which is a particular case of SFG when the two incident fields have identical frequency (for more details see Figures 2 and 3 and the text below).[90] Second order susceptibility is zero for centrosymmetric materials making SHG and S/DFG particularly suited for the study of interfaces and surfaces. S/DFG (Figure 2) involves the annihilation of two input photons at frequencies ω_1 and ω_2, accompanied by the generation of a photon at frequency ω_3.[90]

As already mentioned, SHG is one of the oldest[2] and most popular 2^{nd} order NL techniques (Figure 1). It is a special case of SFG in which the two incoming beams have identical frequencies, and is commonly used in the optical-domain to probe surfaces and interfaces, either statically or dynamically.[91–94] Going into a resonance in SHG or S/DFG enhances the efficiency of the process, while providing spectroscopic identification.[95] By tuning one of the incoming fields over a vibrational or electronic transition, and detecting its mixing with a second incoming field, one can identify the species involved in the dynamics.

Different from $\chi^{(2)}$, the $\chi^{(3)}$ tensors have non-zero elements for any symmetry and each element consists of 48 terms, representing different sequences of the matter density matrix along the process, even though in some cases $\chi^{(3)}$ is determined by only a few dominant contributions due to symmetry.[96] Four-wave mixing (FWM) is a NL third-order process whereby three coherent electromagnetic fields having frequencies $\omega_{1,2,3}$ and wave vectors $\vec{k}_{1,2,3}$ interact with a sample to generate a fourth field (ω_4, $\vec{k}_4$), coherently couple to the three input fields (see figure 1).[89] Each of the three fields induces the sample polarisation vector ($\vec{P}$) to oscillate at its frequency ω_i (i = 1–3), and the excited sample then radiates with a certain phase shift. The interference of the three fields causes beatings at $\omega_4 = \pm\omega_1 \pm \omega_2 \pm \omega_3$, which drive $\vec{P}$ and can be regarded as the radiation source that gives rise to the FWM process. This multiplicity of interactions,[89,90] makes FWM suitable for studying different types of excitations. In FWM, the field $\vec{E}_4(\omega_4, \vec{k}_4)$ is generated by $\vec{P}_3$, which reflects the coupling between the four waves:

$$\vec{P}^{(3)}(\vec{r}) = \chi^{(3)}\vec{E}_1(\omega_1, \vec{k}_1)\vec{E}_2(\omega_2, \vec{k}_2)\vec{E}_3(\omega_3, \vec{k}_3)\exp[\mathrm{i}\vec{k}_4 \cdot \vec{r} - \mathrm{i}\,\omega_4 t], \quad (2)$$

where $\vec{k}_4 = \pm\ \vec{k}_1 \pm \vec{k}_2 \pm \vec{k}_3$ is the phase-matching (momentum conservation) condition. Equation (2) provides insights into the measured homodyne FWM signals ($|E_4(\omega_4, k_4)|^2$), which are proportional to $|\chi^{(3)}|^2$, $|E_i|^2$ (i = 1–3) and their phase factors. The latter indicates that an efficient coupling between the four waves only occurs along a specific direction (see figure 1 bottom), defined by $\vec{k}_4$. Along this direction, the emission from different portions of the excited volume can interfere constructively, as long as the coherence length of the FWM process (L_{FWMc}) exceeds the characteristic dimensions of the interaction volume.[89,97,98] The latter is defined by the overlap region of the fields while $L_{FWMc} = \pi/\Delta\vec{k}$, where $\Delta\vec{k}$ is the wave vector mismatch with $\vec{k}_4$.

This collective response of the system to the input fields leads to a remarkable increase of the NL signal compared to its linear counterpart, which may even become dominant for extended samples. To date though, it still remains unclear, if this behaviour, that is well-known in the optical regime, is retained for shorter wavelengths. The specific direction of the FWM signal ensures a high signal-to-noise ratio. FWM is the basis of several coherent NL methods, such as coherent Raman scattering, Transient Grating (TG) spectroscopy, multi-dimensional (MD) spectroscopy, and impulsive stimulated Rayleigh, Brillouin and Raman (ISRS) scattering (see Figure 1, bottom). These methods involve the generation of dynamic (transient) gratings due to the periodic modulations of the sample's optical properties by different excitations that ultimately drive the time evolution of the excitation gratings.

Coherent Raman scattering (CRS) is a multi-photon technique based on Raman-active vibrational modes of molecules. The two major techniques in CRS are stimulated Raman scattering (SRS) and coherent anti-Stokes Raman scattering (CARS), which were theoretically predicted and experimentally realized in the 1960s.[99,100] They have ever since been extensively used in fundamental studies and from the beginning of the 1980's, their use in microscopy has successfully been implemented.[101]

TG spectroscopy is based on the creation of an excitation grating (of charge carriers, chemical species, heat, magnetism, etc.) when two pulses of identical wavelength λ but with different wave vectors impinge on the sample at t=0 (Figure 1). The decay of the excitation grating is then monitored by means of a third pulse that is detected background-free in a direction determined by the phase-matching condition. In TG spectroscopy, the grating period is given by $L = \frac{\lambda}{2\sin\theta}$, where λ is the wavelength of the incident beams and 2θ their crossing angle. Using shorter wavelengths enables smaller grating periods, going from microns in the visible to sub-nm in the hard X-ray regimes (Table 1). The disappearance of the excitation grating is often due to diffusion, which has made TG the method of choice for measuring dynamics and transport properties in solids, liquids, or gases, with controllable momentum-transfer and background suppression.[102]

TG spectroscopy is a foregoing step in the implementation of MD spectroscopies, which were initially developed for nuclear magnetic resonance (NMR) spectroscopy in the 1970s,[103] and have since then been extended into the optical domain[104] in the infrared,[105] the visible[106–108] and the ultraviolet.[109–111] In these spectroscopies, the two initially incident pulses have a broad spectral range (or are tuneable over a broad range) and are time delayed with respect to each other. The time-domain measurements can be Fourier-transformed into frequency-domain spectra, which are functions of multiple time delays. These spectroscopies enable the simultaneous observation of multiple chromophores and/or transitions in a system, and their evolution with time, which may reflect cross-talk between chromophores. Extending them into the region of core-level transitions would enable the monitoring of time-evolving interaction with element-selectivity between atoms within a given system. This aspect will be discussed in the Outlook section.

The capabilities of short-wavelength NL methods started to be considered over half a century ago, in particular, X-ray/optical wave mixing.[112–118] The process is akin to optically modulated X-ray diffraction in which X-rays scatter inelastically from optically induced charge oscillations and therefore, probe optically polarised charge. The first experimental realization of NL X-ray methods was achieved in the early 1980s as hard X-ray to EUV parametric down-conversion (PDC) using an X-ray tube as source![119] However, theoretical studies were systematically undertaken from the early 2000s.[120–127] One of the first attempts aimed at demonstrating FWM at EUV energies was carried out using an HHG source.[128] With the advent of XFELs, several developments have made it possible to implement NL EUV/X-ray experiments, as discussed below.

Extending NL science into the short-wavelength regime brings several advantages in terms of accessible core-transitions, spatial resolution and momentum transfer (in the case of TG spectroscopy), that are summarised in table I. Depending on the element, the various spectral regimes access different core-transitions, such as the M-edges of 3d transition metals for the EUV, the K-edges of light elements (C, N, O, …) or the L-edges of 3d transition metals in the soft X-ray range, and the K- and L-edges of metals in the hard X-ray range. In addition, heterodyne detection[129,130] should be possible, which will enable disentangling the amplitude and phase terms of a signal, and therefore retrieve the real and imaginary components of the NL susceptibilities in the EUV/X-ray range.

III. APPLICATIONS

III.1 Two-photon absorption (TPA) and Transient absorption:

Two-photon absorption (TPA) was one of the first NL techniques enabled by the birth of the laser.[1] The EUV/X-ray domain involves a rapid decrease of NL susceptibility, e.g. going from visible frequencies to keV photons implies at least a 1000-fold decrease of the TPA cross-section.[123] In addition, it is not even clear whether hard X-ray TPA is dominated by the same

mechanisms as in the optical or even, soft X-ray domains. Because higher-order NL processes require intense X-ray pulses, this implies strong single-photon and sequential multiphoton processes, creating highly charged states. XFELs (due to their high fluxes) and HHG sources (due to their As-pulse durations) enable the high peak powers needed to compensate for the low NL susceptibility. Because of its selection rules, TPA accesses partially or fully dipole-forbidden transitions, which provide information complementary to that obtained using one-photon X-ray absorption. Short-wavelength TPA can also act as an instantaneous probe of excited-state dynamics with chemical specificity, as well as providing better sensitivity for K-shell spectroscopy to connect to the d-states, as discussed later.

Early TPA studies were carried out in the EUV at FLASH,[131] then at the LCLS in the soft X-ray regime[123,132] on rare gas atoms. NL processes competing on the Auger time scale were observed: two-photon, one-electron direct ionisation and two-photon, two-electron sequential ionisation involving transient excited states. The TPA cross-section was found to be 2-3 orders of magnitude larger than theoretically predicted (non-resonant perturbative scaling[133] or second-order perturbation theory[134]), and were attributed to contributions from near-resonant states.[135]

In the hard X-ray regime, TPA was reported at 5.6 keV on Germanium at SACLA.[136] The detected signal was the Ge K_α emission, which can be excited by photons above 11.1 keV. The authors concluded that TPA competes with single and sequential multiphoton processes as in atoms,[123,131,132] and the results were consistent with non-resonant hydrogen-like Z^{-6} scaling. This was confirmed in an experiment on Zirconium at SACLA that used a nanometer-scale focal spot near 9 keV, half the photon energy of the Zr K edge.[137] Upon illuminating Fe and Cu metal foils with intense X-ray pulses near their respective K-edges, Haber et al[126] reported emission at nearly twice the incoming photon energy, which showed a quadratic dependence with the incoming intensity, typical of TPA.

As indicated earlier, sample damage occurs, mainly caused by one-photon absorption due to the high incident fluences required for TPA. Using lower pulse energies and fluences than in ref.[137], and a shorter pulse duration and more efficient detection at SACLA, Tamasaku et al[138] reported the pulse energy dependence of TPA in metallic copper, by detecting the Cu K_α emission.

Saturable transient absorption (STA) is a NL pump-probe technique that exhibits a reduction in the relative absorption of the sample (i.e. an increase in transmission) with increasing incident light intensity. STA is strongly intertwined with TPA and, depending on the resonances, one or the other process becomes overwhelming. This phenomenon has widely been demonstrated in the visible and infrared ranges,[139] and saturable absorbers play a key role in passive mode-locking of femtosecond laser oscillators.[140] Because STA is highly sensitive to the electronic states of the material under study, it is often used as a probe of dynamics and recovery in pump-probe experiments. For example, it has been used to investigate exciton-exciton annihilation,[141] or charge carrier dynamics and diffusion.[142]

Optical-domain STA involves valence electronic states, while in the EUV/X-ray range core transitions are involved, offering the possibility to investigate the underlying processes with element-selectivity. Such studies have been reported at XFELs where the STA of the L-shell transition of aluminium was observed with photon energies of 92 eV (13 nm),[143] followed by observations at the tin N-edge at 24 eV (52 nm)[144] and in the hard X-ray range, at the iron K-edge at 7.1 keV (0.17 nm).[145] In these studies, STA was attributed to depletion of the ground state by the intense pulses, leading to X-ray induced transparency. The intensity threshold for the latter depends on the core transition energy. Transitions from deeper core shells have smaller core-hole lifetime, thus increasing the intensity necessary to observe STA. In a recent study, Hoffmann et al[146] investigated graphite films using soft X-ray FEL pulses of varying intensity. With the help of simulations, they concluded that at lower intensities the NL contribution to the absorption is dominated by STA, due to ground-state depletion, but for higher intensities (>10^{14} W/cm^2), TPA becomes dominant.

While the feasibility of TPA and STA in the EUV/X-ray is now established, further studies would be needed to expand their range of applications.

III.2 Stimulated X-ray Emission/Raman processes

X-ray emission and X-ray Raman spectroscopy can provide information about the energy and dispersion of the elementary low-energy excitations (vibronic, charge, magnon and orbital excitations). The low emission yield of these techniques calls for intense XFEL excitation pulses with, just as for TPA, risks of sample damage. This can be circumvented by stimulating the process with a second pulse.

Stimulated emission from a single X-ray fluorescence line in a Neon gas was reported shortly after the advent of XFELs.[147] Soon after came the demonstration of stimulated X-ray emission from a solid-state sample at the FLASH XFEL under non-resonant silicon L-edge excitation at an energy of 115 eV.[148] The latter produces regions with high 2p-core excitation densities. The spontaneously emitted radiation from recombination of the 2p-core holes (photon energy of 85 eV to ~100 eV) seeds the stimulated emission of soft X-ray photons. The emission spectrum is determined by a spontaneous process as in a typical resonant inelastic X-ray scattering (RIXS) or X-ray emission spectroscopy (XES) and thus, it conserves all the information and specificity of these methods. By carefully choosing the geometry, the weak fluorescence signal was significantly enhanced at the expense of Auger decay, implying a minimised electronic damage to the sample. More recently, Jonnard et al[149] reported stimulated EUV emission from solid magnesium oxide (MgO) at FERMI. In the hard X-ray regime, Yoneda et al[150] reported a hard X-ray inner-shell atomic laser with a copper target pumped by FEL pulses. The dependence of the output energy versus the pump pulse energy, detected in transmission geometry, exhibited a NL enhancement from a pumping threshold, typical of amplified stimulated emission (ASE).

K-shell excitation leads to the K_α, K_β and K_{VtC} (valence-to-core) emission lines. K_α, K_β emission carry information about the electronic and spin structure of the system, while K_{VtC} additionally

contains exquisite fingerprints of the chemical bond of the atoms with their neighbours, their oxidation state, the covalency, etc.[151] However, K_β lines are typically an order of magnitude weaker than K_α lines, while K_{VtC} lines are 2-3 order of magnitude weaker than the K_α lines. Time-domain spontaneous K_α and K_β emission have already been used to probe molecular dynamics with fs-resolution,[152–154] while K_{VtC} emission was observed with ps-resolution at synchrotrons,[155] and more recently, with fs-resolution at XFELs.[156] By externally stimulating the K_β or K_{VtC} transitions, one could enhance the sensitivity of such experiments. In a recent article, Kroll et al[157] reported the observation and analysis of the gain curve of amplified K_α emission from solutions of Mn(II) and Mn(VII) complexes, finding spectra at amplification levels extending over four orders of magnitude until saturation, and bandwidths below the Mn 1s core-hole lifetime broadening in the onset of the stimulated emission. In a more recent work, they also reported observation of seeded amplified K_β emission from a $NaMnO_4$ solution using two-colour XFEL pulses, the first creates the 1s core-hole population inversion and the second seeds the amplified K_β emission. The latter showed a signal enhancement of > 10^5 with respect to the conventional K_β emission, within the same solid angle. The upcoming As XFEL pulses[158] promise to beat the core-hole lifetime and drive the system into amplification of specific emission lines.

Femtosecond stimulated Raman spectroscopy is a NL optical method that has successfully been implemented for the study of vibrational dynamics with high spectral and temporal resolution.[159,160] In the X-ray regime, resonant inelastic X-ray scattering (RIXS)[151,161–163] is an ideal tool for populating electronic valence states that are inaccessible by direct excitation in the UV-visible. Stimulated RIXS (SRIXS) has therefore the potential of significantly populating such states[164] and when driven by As-pulses, it would allow a direct probing of valence electron wave packets[122,165,166] or of coupled nuclear-electronic motion on As-timescales.[167]

SRIXS was first achieved for atoms,[168,169] and more recently in diatomic molecules such as CO[170] or NO.[171] The use of As X-ray pulses was shown to induce electronic population transfer via SRIXS using the broad spectral bandwidth (5.5 eV full width at half maximum). The impulsive excitation was resonantly enhanced by the oxygen 1s → 2π* resonance of nitric oxide (NO), and the excited states of the neutral molecules were probed with a time-delayed UV pulse.

Stimulated resonant elastic (SREXS) and inelastic (SRIXS) X-ray scattering were recently reported near the cobalt L_3 edge (770-785 eV) in solid Co/Pd multilayer samples. A 4 to 5 orders of magnitude enhancement of the stimulated over the spontaneous RIXS signal was reported.[172] However, for both signals, contributions from inelastic electron scattering processes were observed, even for very short pulses. This results in valence electron redistribution effects that distort the stimulated REXS and RIXS spectra due to overlapping spectral changes. Therefore, a detailed characterization of these effects is needed in order to establish stimulated RIXS as a tool for the study of low-lying excitations in solids.

We already mentioned the 2-photon study by Haber et al[126] on Cu and Fe foils, which were excited with photons of energy from just below the relevant single K-shell threshold to well above the sequential double K-shell threshold, and the measurements included higher energy photons below twice the input energy. The spectrum of emitted high-energy photons showed both dispersive and non-dispersive lines that were attributed to double-core hole mediated resonant X-ray Raman, analogous to hyper-Raman scattering, and 2-electron/1-photon fluorescence. This can be considered as an anti-Stokes process from a core-excited intermediate state where the excess energy is taken up by one or more photoelectrons and lines. In all cases, K-shell electrons are excited and subsequently de-excited during the process.

III.3 Sum/difference frequency generation

In the X-ray domain, S/DFG is akin to optically-modulated X-ray diffraction in which X-rays inelastically scatter from optically induced charge oscillations and therefore, probe optically polarised charge. This additionally allows the optically-induced microscopic field to be determined as it is closely related to the induced charge.[173,174] Although the idea has been around for a long time,[112–118] and further theoretical developments have more recently been made,[121,124,125,175,176] the experimental verification of such processes had to await the advent of XFELs.

In a pioneering experiment, Glover et al[177] demonstrated X-ray/optical SFG in a single-crystal of diamond. The observation included the optically modulated X-ray diffraction from the (111) planes that generates a pulse at the sum-frequency of the incident optical (1.55 eV) and X-ray (8 keV) pulses. In order to increase the efficiency and access the atomic-scale motions, the process is phase-matched using a reciprocal lattice vector. The phase-matching geometry determines the direction of the generated photon, slightly offset from the Bragg diffracted beam. This should allow reconstructing the induced charge distribution. The implications of this work are far reaching: it shows that X-ray/optical SFG provides simultaneous access to the induced charges and the associated microscopic fields that arise when light illuminates a material. It also paves the way for X-ray/optical-EUV S/DFG processes to study the ultrafast dynamics at surfaces/interfaces by directly probing valence charges on atomic time and length scales. The information content of such experiments can be considered in close analogy to spontaneous RIXS experiments, but the achievable signal levels should be substantially enhanced in the NL process through the coherent mixing of the involved fields and the associated phase-matching conditions (see Figure 2). However, generalization of optical/X-ray SFG is challenging because of its low efficiency, which depends linearly on the intensity of the optical laser. Therefore, it requires optical intensities that are often larger than the radiation damage threshold of most materials, which in addition need to be optically transparent, therefore limiting the range of systems one can investigate.

We earlier mentioned PDC, which is similar to an X-ray or EUV/optical DFG. In the first such experiment,[119] using the 002 reflection of a LiF single crystal, Danino and Freund observed phase-matched PDC of 8 keV (Cu-K_α) photons from a commercial rotating anode into single

photons at 7.7 keV, with idler photons in the EUV at 335 eV. This was followed by X-ray to EUV PDC studies at synchrotrons[178–180] demonstrating, in particular, that one can visualize the local optical response to EUV radiation with atomic resolution.[180] Extending X-ray PDC to the optical domain could provide a powerful probe of charge oscillations, e.g. in phenomena that are associated with energies near the Fermi energy of metals or near the band gap of semiconductors. This was achieved at a synchrotron by Schori et al[181] who reported X-ray PDC from 11 keV to 4-3 eV photons.

Overall, one of the key advantages of optical/EUV or optical/X-ray S/DFG is the fact that the optical pulse can be tuned to vibrational or electronic transitions, while the EUV/X-ray pulse can be tuned to specific core-transitions. This gives an enhanced flexibility in terms of resonance conditions corresponding to vibrational/electronic transitions and core transitions for systems lacking inversion symmetry. Further enhancement of signals can be achieved using e.g. plasmonics in the case of electronic resonances.

III.4 Second-Harmonic generation

Extending SHG into the EUV/X-ray domain offers the additional advantage of element-selectivity. Furthermore, the theory of X-ray non-linearities in solids[112,113,116] assumes that since all pertinent photon energies are much higher than the binding energies of the electrons in light elements, the electrons can be treated as free particles, and the dominant non-linearity is plasma-like. EUV/ X-ray SHG may thus provide a new window into electron densities in the future. This non-linearity is very different from the optical-domain non-linearities in that it is non-local, second-order, and may be observed in centrosymmetric materials, provided a non-uniform electron density is present.

In EUV/X-ray SHG spectroscopy, the incident beam is resonant or half-resonant with a core-to-valence transition, such that the resulting resonantly enhanced, background-free signal is sensitive to core levels (Figure 3a). By frequency-resolving the SHG radiation, the symmetry breaking can be correlated to particular spectral features. The first demonstration of short-wavelength SHG was made on a diamond crystal using 7.3 keV photons from the SACLA XFEL with 10^{16} W/cm^2.[182] An SHG efficiency of 5.8×10^{-11} was reported. This work was followed by SHG near the carbon K edge (~284 eV) in transmission geometry (Figure 3b) on graphite thin films using soft X-ray coherent pulses at FERMI.[183] The experimental results were accompanied by a theoretical analysis, which highlighted the effect of resonant enhancement above the C K-edge and showed interfacial-sensitivity of the technique in a centrosymmetric sample with the second harmonic intensity predominantly arising from the first atomic surface layer. In another study, Yamamoto et al[184] demonstrated SHG from a non-centrosymmetric bulk crystal of $GaFeO_3$ using pulses from the SACLA XFEL. The XFEL photon energy was set to half of the Fe 3p absorption (M-) edge (~53 eV) and the SHG signals were enhanced by a double-resonance effect met by the O 2s → Fe 3d (inter-band) and the Fe 3p → O 2s (intra-band) transitions (Figures 3c,d). This offers an exciting leverage in the study of transition metal oxides, where it is possible to satisfy the double-resonance between the O L_1- and metal M-

edges, and thus enhance the signal. We note that in contrast to figure 3b, this work was carried out under reflection geometry, for which the wave vectors along the sample surface are required to match, a condition that is automatically satisfied, and the momentum transfer of the sample in the normal direction does not give a critical condition in the regime where the wavelength is larger than the attenuation length. This points to possible applications of the method to a large variety of samples and experimental conditions. The same reflection geometry was also implemented to investigate the broken inversion symmetry in the polar metal phase of $LiOsO_3$ with an enhanced feature above the Li K-edge that reflects the degree of Li atom displacement.[185]

Probing buried interfaces using optical methods can be quite challenging and does not provide element-specific information. Recently, EUV-SHG was used around 190 eV at FERMI to probe the buried interface of a boron film with a support layer of Parylene N, a prototypical organic-inorganic interface. The experiment revealed distinct spectral features that are not observed in X-ray absorption spectra, demonstrating its extraordinary interfacial sensitivity. With the help of electronic structure calculations, the boron-organic separation distance was derived, but most important, they showed that sub-Å changes translated into spectral shifts of the order of 100s meV that are easily detected by EUV-SHG.[186]

HHG sources have also been used to carry out ultrafast SHG experiments in the EUV. Such an experiment was recently achieved above the Ti M edge (32.6 eV) of solid Titanium using high-power HHG sources.[88] Comparison of the observations with density functional perturbation theory (DFPT) and real-time time-dependent density functional theory (RT-TDDFT) calculations suggested resonant contributions from Ti-3p to Ti-3d transitions to the SHG signal at the Ti surface.

What emerges from the above is that while EUV SHG is still interface sensitive, hard X-ray SHG seems to respond to the bulk in the case of non-centrosymmetric crystals. A systematic investigation of such phenomena would widen the range of applications of EUV/X-ray SHG, and even of S/DFG methods.

III.5 Four-wave mixing (FWM):

Extending FWM techniques (Figure 1) into the EUV/X-ray domain allows novel insights into the electronic structure and dynamics of the systems under study.

Prior to the XFEL era, studies with EUV HHG pulses had already demonstrated the coupling of fields either all-EUV as in ref. [128], or optical and EUV pulses.[80,81,83,84,187] In the latter cases, the TG was generated by optical domain pulses and the EUV-HHG radiation was generated by a third optical pulse within the excited fringes. Exploiting the grating to disperse the various harmonics offered an elegant way of monitoring the rotational wave packets of molecular systems[83] since the HHG signal is sensitive to the alignment of the molecule with respect to the laser polarisation. More recently, Leone and co-workers demonstrated an insightful use of FWM by combining an As EUV HHG pulse and two separately timed few-cycle near-infrared

(NIR) pulses,[188] to characterise the dynamics of the Na^+ $L_{2,3}$ edge core-excitons in NaCl. An inhomogeneous distribution of core-excitons underlying the Na^+ Γ-point spectrum was deconvoluted by resonance-enhanced FWM. In addition, dark excitonic states that are coupled to the XUV-allowed levels by the NIR pulses were characterised spectrally and temporally. The coherence lifetime of the core-exciton states was found to be <10 fs.

A recent experiment at FLASH[189] extended a similar mixing of two optical photons with an EUV photon on a LiF sample. Instead of analysing the spatial dependence of the emitted EUV at the same wavelength as the incoming beam, a co-linear scheme of optical laser and EUV FEL was used, but the emitted photons were observed at energies offset from the incoming EUV by two optical laser photons, in both an SFG and a DFG scheme. Strong enhancements of the signal at the Li 1s resonance were observed when either the incoming EUV pulse or the emitted EUV photons hit the resonance. The signal strength increased where the localized excitonic EUV resonances overlapped with an optically induced local resonance, but were below the detection threshold at delocalized band structure features. This result opens a new window into probing the localization degree of excitations in matter using NL spectroscopy and provides an experimental step towards realizing more complex experiments (see Figure 2).

X-ray diffraction has long been used to probe optically-induced TG's at synchrotron-based experiments. The X-ray pulse is capable of probing the grating at a spatial resolution limited by the grating period. The amplitude of transient surface deformations was determined with sub-Å resolution and control of the amplitude and the phase of a thermally deformed surface was achieved.[190,191] This approach has also been used to study photoinduced strain (structural grating) with an amplitude proportional to the optical fluence, as well as magneto-structural phase transformations.[192]

Various short-wavelength FWM schemes have been proposed (figure 1). However, TG emerged as one of the most popular and it offers (Table 1) element-specificity, smaller grating periods in the nanometer scale, large momentum transfers and access into new kinematic regions, hardly accessible otherwise (Figure 6). Indeed, in such experiments, the temporal information about the low-order NL light-matter interaction is mapped into the spatial domain where it can be observed against a zero background.[4] This enables measurements where only a small fraction of the molecules is excited, as is the case for typical diffracted signals (for more details, see Figures 4 and 5 and the text below). In order to fully benefit of the capabilities of EUV/X-ray TG spectroscopy (Table 1), the probe pulse must also be in the EUV or X-ray range, which implies controlling in energy and time two such pulses, a task which is a challenge to this day although solutions are now being implemented. However, prior to that a first major step was achieved by Bencivenga et al[193] who used two ultrashort (60-80 fs) EUV (27.6 nm) pulses from the FERMI FEL to generate a TG on an SiO_2 glass and probed it with a ~100 fs optical beam at 392.8 nm. The results (Figure 5b) clearly show the electronic response at t=0, followed by an appreciable signal up to Δt = 130 ps. For Δt>10 ps, the signal was ascribed to thermal relaxation and longitudinal acoustic modes, while at shorter times (<1.6 ps), coherent

oscillations due to optical (Raman) phonon modes were observed, demonstrating that EUV TGs can drive coherent excitations in the sample, an observation that was confirmed on other systems (see below). As mentioned above, probing an EUV-generated TG with an optical pulse severely limits the spatial resolution. Therefore, in a subsequent experiment,[194,195] the FERMI team demonstrated all-EUV TG (Figure 4a) on silicon or silicon nitride. The third EUV probe pulse was time-delayed with respect to the first two and was of identical energy. Tuning the time between the pump and the probe pulses was carried out using the split and delay scheme shown in Figure 4a. The signal exhibits coherent phonon oscillations on top of a slowly decaying background (Figure 5a). The latter, along with the damping of the oscillations are related to the thermal equilibration time. Most remarkable is the absence of the electronic response peak at t=0, which occurs in the all-optical TG or optically-probed EUV TGs (Figure 5b).[193] This is due to the fact that the refractive index changes at optical wavelengths are highly sensitive to electronic excitations of the conduction/valence band, while at EUV wavelengths they are mostly sensitive to changes in the total electronic density, making the all-EUV TG signal sensitive to the structural response. This offers a way of distinguishing electronic and nuclear responses in materials.

The demonstration of EUV TGs[193,195] led to a flurry of studies on the generation of coherent acoustic and optical phonons,[196,197] the element-specificity of the EUV-generated resonant TG,[198] the probing of thermoelastic properties of materials,[199] and on the generation, control and probing of magnetic patterns.[200,201] The latter three studies used an all-EUV TG configuration. The work on magnetization TGs having periods of a few 10s of nm in a CoGd alloy,[200] was carried out using two pump energies, one resonant with the M-edge of Co, and the other (non-resonant) at half the energy of the first. In both cases, the probing was resonant with the M-edge of Co. It was found that the patterns of a sample magnetised to saturation (by an external static magnetic field) appear on a sub-ps time scale (similar to the electron−phonon relaxation in a metal) as the sample is thermally demagnetized by the EUV-TG, and they decay on time scales of tens of picoseconds, suggesting that thermal transport is the leading mechanism that erases the magnetization grating. The TG period dependence was investigated (Figure 5c), indicating a transport process. Indeed, on the time scales of the decay, the lattice, electronic, and spin systems are in thermal equilibrium, and as the temperature grating is erased by thermal diffusion, the magnetization grating also decays. This result is also a clear manifestation of the effect of the grating periodicity on the transport kinetics.

Going into the shorter wavelength range of hard X-rays opens up an even smaller range of nanoscale periods (Table 1) for which the nature of transport is unknown and in particular, the cross-over from ballistic to diffusive transport. The challenge in this spectral domain is the lack of reflective optics. In order to circumvent it, Svetina and co-workers[202,203] used diffractive optics, namely the Talbot effect (Figure 4b). They first demonstrated the formation of permanent gratings on solid samples using 3 keV photons from the Swiss Free Electron Laser (SwissFEL).[203] Thereafter, they created a TG in BGO at 7 keV, which was probed by an optical

pulse at 400 nm.[202] This experiment demonstrated hard X-ray TG with the signal (figure 5d) exhibiting the same optical phonons as in the non-resonant EUV-TG experiment discussed above.[196] While in the latter they were attributed to a displacive excitation and in optical experiments to ISRS,[204] the mechanism in the case of hard X-rays is yet to be determined.

More recently, Peters et al[205] achieved hard X-ray TG generation by crossing two X-ray 30 fs beams generated by an X-ray split-delay line (Figure 4a) at LCLS[206] and probed it by an optical pulse. Their result opens the possibility to delay one of the two pump pulses and perform FROG detection of X-ray TG measurements. This development is important in view of multidimensional core-level spectroscopy.

A recent experiment showed that hard X-rays can interact and even manipulate magnetic orders, e.g., domains, just as EUV radiation, but with the advantage of smaller grating periods down to a few nanometers.[207] Manipulation of magnetic domains by impinging high intensity permanent gratings at 7 keV in thulium-substituted Yttrium Iron Garnet (Tm:YIG) sample with perpendicular magnetic anisotropy was achieved. This experiment also indicates that by reducing the X-ray flux, transient excitation of magnetic orders, such as magnons, can be triggered and subsequent dynamics can be probed at the characteristic scales of the collective excitations. While dealing with permanent gratings, this experiment implies that magnetic TG's could also be generated using hard X-rays with nanoscale periods.

Recent experiments have demonstrated hard X-ray TG in solutions and all Hard X-ray TG in solids, and the results are being analysed at present.

IV. Theoretical developments

The above emerging NL experimental capabilities and their advances call for robust theoretical and computational tools that should help model and support the interpretation of signals, as well as inspire new innovative experiments.[208] These studies operate either in the static regime, developing and utilising efficient and accurate electronic structure theory methods for the calculation of core-hole states,[209–212] or in the time-dependent regime by the calculation of molecular dynamics by different numerical methods.[213–218] Theoretically, the computation of time-resolved X-ray signals poses challenges such as the accurate and efficient calculation of core-excitation energies.[210–212,219–224] These are required to pre-screen possible experiments and make optimal use of the precious beam time.

As mentioned earlier, the idea to probe optically-induced charge distributions via optical/X-ray wave-mixing dates back to the 1970s.[112–114,118,225] Further to this, the experimental realizations of X-ray PDC to EUV[119,178–180] or to UV-visible[181] photons have convincingly been interpreted by theoretical models.[178–181,226] These models are complementary to those used for the analysis of optical/X-ray S/DFG.

Finally, the advent of the XFELs also initiated theoretical work aimed at interpreting the first results that were obtained, essentially on the multiphoton processes in atoms, yielding good agreement with experiments.[227,228,123,132,135,229,230] Significant theoretical efforts have been made over the past 10-15 years aimed at exploring and proposing new innovative experiments

enabled by the capabilities of XFEL and HHG sources. Some of these are discussed in the next section, along with the possible future directions in techniques and methods of the field.

The success of optical/X-ray SFG[177] at an XFEL prompted renewed theoretical activity in this area. Gorelova, Santra and co-workers[126,127,231,232] have developed a general theoretical framework to describe the interaction of general Floquet systems with an X-ray pulse. Floquet theory is used to describe the laser-driven electronic system. The scattering probability of an arbitrary non-resonant X-ray pulse from such a system is then obtained employing the density-matrix formalism. These studies show how the time-dependent electron density of a crystal can be reconstructed from energy-resolved scattering patterns.

Careful inspection of the multipoint correlation functions appearing in the expression of time-resolved X-ray diffraction signals shows that diffraction also occurs from coherences on top of the usual population contributions.[233,234] The diffraction from coherences is usually neglected because it does not scale with the total number of electrons in the system like the population terms (Figure 7), but rather depends on the few electrons involved in an optical transition. However, it is of interest to extract the coherence terms from the signal since they contain direct information on the motion of the charges at any given time. These provide new signatures of elementary dynamical phenomena in molecules and solids[227,228,235–241] such as electronic coherence created at conical intersections (CoIns),[242] evolving electron and nuclear densities and structural changes. Some of these, dwelling on molecular systems, are summarized in Figure 7 together with their loop-diagrams corresponding to the (multi-point) correlation functions required for their numerical computation.

The simplest way to access them is to perturbatively disturb the molecular system with an optical field, and at the first order in this actinic field, this corresponds to a two-point correlation function of a dipole operator and the charge density operator. Since the charge density interacts with the square of the field vector potential $\mathbf{A}^2$, the signal is reminiscent of an SFG process from the field perspective, discussed in § III.3 and the signal is named X-ray Sum Frequency diffraction (Figure 2).[240] In a more general perspective, the actinic excitation can be treated non-perturbatively, typically numerically, leading to the more general ultrafast X-ray diffraction signal of non-equilibrium states only accessible by ultrabright, femtosecond XFEL pulses.[23]

Serrat used real-time time-dependent density functional theory simulations and extended DFG to the resonant case (so-called Resonant-DFG or Re-DFG) into core-transitions of specific atoms in a molecular system.[124,125] Compared to the third-order stimulated Raman process (XSRS), re-DFG is a parametric process, and as such it does not excite the molecule. The expected re-DFG signal strength is estimated to be stronger than the competing XSRS process.

V. Outlook

The above survey of ultrafast EUV/X-ray NL theoretical and experimental techniques shows the rich perspectives they offer in terms of fundamental Science, as well as applications. In

the following, we dwell on the current technical, methodological and theoretical developments and how they can shape the future of the field.

Source and Methods development:

a) Sources

Just as for the optical domain, the birth and development of non-linear EUV/X-ray science has been enabled and will expand hand-in-hand with that of instrumentation. In return, the strong drive towards these methods is motivating several upgrades at existing XFELs aimed at improving the emitted pulse features ranging from the time duration to the spectral purity and from the repetition rate to the multi-colour production. Besides the external seeding upgrades mentioned above, SASE FELs are moving towards self-seeding schemes[243] providing more energy stable pulses having durations of 100s of As but with random intensities.[158] The upgraded LCLS-II machine promises a major jump in capabilities thanks, among others, to the increased repetition rate from 120 Hz to the MHz regime,[244] which will bring enhanced signal-to-noise ratios.

Many of the theoretical schemes[165,168,169,245,246] (vide infra) proposing stimulated X-ray Raman, emission and/or multidimensional X-ray spectroscopy rely on the use of spectrally broad As-pulses that would in addition need to be phase-locked and temporally controlled. The experimental demonstrations of stimulated X-ray Raman and emission are materialising these predictions and showing the way to go.[148,170–172,247]

An important goal to enhance the use and applications of NL EUV/X-ray methods is to make them more accessible by developing smaller, table-top systems. HHG sources are making strident progress in terms of repetition rate, energy/pulse and stability and have started to be used in these respects.[25,27,88] Their ultrashort durations means high peak powers, which should favour 2nd order processes, such as TPA, while minimising sample damage due to one-photon absorption.

In addition, there are major efforts at developing compact and economic accelerators. A new acceleration technology that could reduce the size of particle accelerators is plasma wakefield acceleration.[248] Laser wakefield accelerators can sustain accelerating gradients more than three orders of magnitude higher than those of the current (radio-frequency based) accelerators, and are considered an attractive option for driving compact XFELs. The realization of such devices remains a challenge owing to the relatively poor quality of electron beams that are based on a laser wakefield accelerator. Nevertheless, amplified undulator radiation at 27 nm has recently been reported, with around 10^{10} photons per pulse.[249] A demonstration was made showing infrared FEL radiation with the typical exponential growth of its energy over six consecutive undulators.[250] Compared to SASE, the seeded FEL pulses have energies 2 orders of magnitude larger and a 3 times higher stability. The seeded configuration was also demonstrated at 270 nm with control over the radiation wavelength.[251]

b) Pulse characterization

TG can also be implemented to characterize ultrashort pulses overcoming limitation of the instrumentations' electronics which are too slow. This is routinely done in the optical regime by frequency-resolved optical-gating (FROG) methods where, by spectrally resolving a NL signal as a function of time delay, it is possible to obtain fs/as resolution thanks to the radiation – matter interaction that provides an ultrafast "shutter".[252] In a recent study, TG-FROG was applied at FERMI[253] to measure the pulse length and coherence on a shot-to-shot basis by means of EUV-TG and optical probe on a slowly responding medium as sample (a Si_3N_4 film) thus, not only demonstrating the applicability of the method at short wavelengths, but also providing a valuable tool to characterize EUV HHG and FEL pulses.

c) Multidimensional Covariance signals

Most NL spectroscopy protocols were originally designed for coherent, phase-controlled pulses. While seeded FELs at XUV frequencies such as FERMI do provide coherent pulses,[32,254,255] soft to hard X-ray FELs mostly rely on noisy SASE pulses.[32] Their stochastic nature (see § II.1) represents a bottleneck for the implementation of NL spectroscopies that require reproducible, phase-controlled X-ray pulses.

Correlation methods, based on, e.g., a covariance analysis or ghost imaging, represent a promising route to overcome this issue and retrieve information from noisy stochastic signals.[170,256–259] These methods exploit the fact that each measured signal is uniquely related to the FEL pulse generating it. They have been proposed to record so-called TRUECARS signals, which are discussed below.

Spectral covariance methods can be extended to a broad range of time-resolved X-ray signals, so long as different frequency-dispersed observables, such as the incident and transmitted pulse intensity profiles, can be measured and correlated. For instance, a correlation analysis of the frequency-resolved diffraction signal would allow separating elastic and inelastic diffraction patterns, and thereby imaging the motion of the electrons directly involved in molecular dynamics.[256] This thus motivates the development of new detection methods, as well as improvements in the characterization of the X-ray pulses available at FEL sources.[260,261]

Open questions and future developments:

It is difficult to condense in a short text the innumerable possibilities offered by the development of NL X-ray/EUV science. In the following, we will discuss a few experimental and theoretical cases and also the pending questions that need to be solved if we want to expand the use of the current methods described above.

a) <u>Surface and interfaces processes:</u>

There is an acute need to probe photo- or electro-catalytic processes at surfaces or at buried interfaces, e.g. in batteries, and several *in-operando* schemes[262–264] exist, which usually combine a wide variety of methods (ambient pressure UPS, XPS, electron/X-ray diffraction, X-ray absorption/emission spectroscopy, AFM, optical SHG/SFG/DFG, etc.) making them complex and at times, difficult to interpret. The holy grail of these efforts is to achieve

element-selectivity. The capabilities opened up by SHG and S/DFG in the region of core-transitions (eventually combined with valence excitations for S/DFG) offer an unprecedented approach to probe processes ongoing in systems such as heterojunctions and non-centrosymmetric materials with element-selectivity, surface-specificity, ultrahigh temporal resolution and under ambient conditions. They have the potential to become routine methods for the characterization of catalytic processes, even in the lab as SHG has been demonstrated using HHG sources.[88] Such studies could be further extended to biological surfaces (e.g. membranes) in order to, e.g. probe ion exchanges therein.

X-ray/optical S/DFG processes can be regarded as the coherently stimulated inversion of a spontaneous X-ray decay into a low-energy excited state (see Figure 2a).[265] While first order X-ray/optical mixing has been demonstrated,[177] we mentioned another level of insight into the charge distribution that can be gained by mixing the X-ray photon with an integer number $n > 1$ of optical photons to generate a photon with energy that is the sum (or difference) of the energies of the incoming X-ray and optical photons (Figure 2b).[189] Measuring multiple Fourier components for both the first and second order scattering processes, i.e., for the mixing of one (n=1) or two (n =2) optical photons (respectively) have been calculated[266] for the optically-induced charge distribution in a GaAs unit cell (Figure 2c), predicting the feasibility of such experiments. Higher order studies can deliver new views on functional matter where the dynamics of low-energy excitations determine the interaction with the environment, like a response to external perturbations that is reflected in changes of the electronic properties. Applications range from information technology for data processing and storage to highly-specific sensing devices.

b) <u>Chirality:</u>

Chirality remains one of the most challenging issues in applied spectroscopy because of the demand by the pharmaceutical and chemical industries. The most used method is circular dichroism (CD) spectroscopy, which has intrinsically weak signals (typically 0.1 % of the total absorption). Going into the X-ray domain enhances, in principle, the signals as the higher order terms of the light-matter interaction Hamiltonian scale as a/λ where a is the molecular size and λ the radiation wavelength, and it offers element-selectivity. While efforts are on-going to implement steady-state and time-resolved linear X-ray CD (but also helical dichroism),[267–272] further enhancements in signal intensity and selectivity could be reached by moving to the NL regime.

It was found in the 1990s that optical-domain SHG exhibits large chiral-specific responses on thin films and macromolecular assemblies.[273–277] Furthermore, theoretical and experimental studies have confirmed the viability of detectable SFG signals in isotropic chiral media.[278–282] Implementing X-ray SHG, Optical/EUV or optical/X-ray S/DFG would provide a further degree of selectivity both on the optical side (vibrational or electronic excitations) and the EUV/X-ray side (core-transitions).

Chiral crystals have a lattice structure that has a well-defined handedness due to the lack of inversion, mirror or other roto-inversion symmetries. They are often topological solids in that the bulk is insulating while the surface is conducting. Their electronic structure is the subject of intense investigations,[283–285] but it remains largely uncharacterized. Using Optical/EUV or optical/X-ray S/DFG with circularly polarised pulses would greatly help unravel their topological electronic properties, in particular when it comes to higher-fold chiral fermions.[285] Theoretical developments would need to be developed in parallel to fully describe their electronic structure.

In the mid-1990s, Terazima has proposed to use TG to enhance the detection of CD.[286] His idea consisted in creating a TG using two beams linearly polarized at 90° of each other, which would create a circularly polarized excitation grating that can then be detected background-free by a third probe pulse (Figure 1), i.e., only the difference in absorption is detected as the TG signal. The recent achievements in the field of EUV/X-ray chirality[271,272,287,288] and EUV/X-ray TGs[193,200,202,289] are offering promising prospects to such studies.[290] In addition, NL chiral signals offer a way to control which chiral pathways contribute to the final signals by using various polarization and pulse geometry configurations.[291] X-ray Raman Optical Activity can already be considered a 4th-order NL process involving two interactions with the incoming beam and two interactions with the spontaneously emitted photons.[287] When four classical fields are involved, it is possible to design a large class of chiral X-ray 4WM techniques (see Figure 7b).[290,291] Numerous pseudo-scalars can be constructed from four-point-correlation functions and the irreducible tensor formalism proves useful to categorize the set of all independent combinations of incoming beam polarizations needed to extract them. Such techniques have the advantages of NL X-ray techniques such as Stimulated X-ray scattering (e.g. probing a large manifold of state with a single technique) combined with the sensitivity of inversion breaking of chiral signals.

c) <u>Conical Intersections:</u>

Using stimulated X-ray Raman and X-ray emission, the corresponding signal levels can be substantially enhanced, especially due to the formation of a directed emitted beam that carries all the information and can be very efficiently detected background-free. Furthermore, the delivery of As-pulses at XFELs allows to beat the core-hole lifetime and further enhance the stimulated signals. Such experiments could thus preserve the deep information content of RIXS, but the higher signal levels enable access to new parameter spaces (like external fields, chemical compositions, pressure etc.) where systematic studies were inhibited by overwhelming acquisition times. Beyond this, novel schemes have been envisioned that exploit these stimulated signals to address outstanding scientific questions, as outlined hereafter.

An elementary molecular process that has received much attention is the passage through CoIns, where adiabatic states become degenerate and electronic and nuclear motions become strongly coupled, opening ultrafast, non-radiative relaxation channels that can either go back

to the reactant geometry or lead to photochemical pathways that generate new products, otherwise not accessible in the electronic ground state. Ultrafast CoIns thus determine the outcome of photo-induced processes, such as the primary event of vision[292,293] and the photostability of DNA nucleobases against UV radiation.[294] Their spectroscopic detection remains a formidable challenge because it requires precise temporal resolution and a broad, few-eV observation bandwidth. Ultrafast XAS and XES have been proposed as tools for their detection,[241,295–298] such that the temporal and spectral profiles of the CoIn passage are read off by the changes in the absorption/emission lines with the pump-probe delay encoding the system's dynamics. While efforts are on-going in this direction,[70,299,300] a probe of electronic coherence emerging at CoIns, the so-called Transient Ultrafast Electronic Coherences by As Stimulated X-Ray Raman Signals (TRUECARS) has been proposed.[237,239,245] It consists in tuning the X-ray probe pulse off-resonant to any material transition and inducing a stimulated Raman process between electronic states (see Figure 7a). No probe photon is absorbed, but the spectrally dispersed probe pulse exhibits an energy redistribution upon interaction with the molecule, stemming from Stokes and Anti-Stokes Raman processes and leading to characteristic gain and loss features in different spectral regions. This signal requires electronic states to be in a coherent superposition, facilitated by CoIns through wave packet bifurcation and subsequent population of both electronic states (Figure 7). The signal is background-free from state populations that dominate the transient absorption signal and would provide an unambiguous and direct probe of CoIns, and has proposed to monitor CoIns in nucleobases,[237,301] bichromophoric molecules,[233] and dendrimers.[302] Efforts at implementing it experimentally are on-going.

The above-mentioned multidimensional covariance was exemplified for TRUECARS, which requires phase-controlled pulses, but it would be similarly applicable for other frequency-resolved signals. For stochastic FEL pulses lacking phase control, the TRUECARS signal averaged over independent repeated measurements is expected to vanish. However, spectrally and temporally resolved information can be retrieved by an analysis of the spectral covariance $\mathrm{C}(\omega_{\mathrm{in}}, \omega_{\mathrm{out}}, \mathrm{T}) = \langle \mathrm{I}_{\mathrm{in}}(\omega_{\mathrm{in}}) \mathrm{S}(\omega_{\mathrm{out}}, \mathrm{T}) \rangle - \langle \mathrm{I}_{\mathrm{in}}(\omega_{\mathrm{in}}) \rangle \langle \mathrm{S}(\omega_{\mathrm{out}}, \mathrm{T}) \rangle$ between the signal $\mathrm{S}(\omega_{\mathrm{out}}, \mathrm{T})$ and the incident pulse intensity $\mathrm{I}_{\mathrm{in}}(\omega_{\mathrm{in}})$. This two-frequency covariance map provides information by exploiting the correlations between the spectral components of the stochastic pulse and for TRUECARS, it was shown to offer the same depth of physical information one could obtain with phase-controlled pulses.[245] The implementation of covariance methods at FELs requires knowledge of the field's correlation properties, such as the n-point spectral correlation functions.[260]

d) <u>Nanoscale transport</u>

EUV-TG methods are now well-established tools to probe the lattice, electronic, and magnetic dynamics of materials. The ability to tune the grating period offers a window of opportunities for the study of various nano- to mesoscale transport phenomena (Figure 6), provided an all-EUV geometry is used.[195] The nanoscales are hard to reach with present day methods, except in a few rare cases,[303] however the demonstration of hard X-ray TG[202,203] allows to break into

this length scale, provided an all X-ray TG configuration is adopted. This capability is being expanded at present in order to probe the nm-grating periods with adequate resolution. Experiments have been carried out at SACLA and LCLS and the data are being analysed. The extension of hard X-ray TG to (bio)chemical systems would offer access to short-range electron[110] and energy transfer[304–306] processes in biosystems as well as to chemical dynamics and diffusion in solutions. Regarding the latter, an experiment was recently carried out at the SwissFEL making a TG at the Fe K-edge of ferrioxalate in an aqueous solution,[76] which was probed with 800 nm and 400 nm pulses. Analysis of the data is underway. Further extensions into the all X-ray TG is envisioned.

The full exploitation of short-wavelength TG techniques calls however for a convincing demonstration of its element-specificity. This is also a necessary condition for the extension of EUV/X-ray TG towards multidimensional spectroscopies. So far the studies reporting effects due to specific core-transition edges[198] reflect the increased absorption coefficient at the edge, but no genuine dynamics launched via excitation of specific atoms. A corollary to this issue is the generation mechanism of the excitation. The EUV TG-generated optical phonons of Bismuth Germanate ($Bi_4Ge_3O_{12}$ or BGO)[196] at 2.7 THz were also observed in the hard X-ray TG experiment (Figure 5d).[202] These coherences had been generated by optical Impulsive stimulated Raman scattering experiments (ISRS)[204] and attributed to a displacive excitation.[307] The fact that they appear in all three types of experiments calls for an understanding of the generation mechanism of these phonons if one wants to exploit EUV or X-ray TG for manipulating and controlling the dynamical properties of materials.

EUV TG is the equivalent of a time-domain EUV Brillouin scattering experiment, which replaces the non-existing EUV spectroscopic Brillouin scattering. As such, EUV TG experiments can fill the gap between optical and X-ray or neutron Brillouin scattering (Figure 6). All-EUV TG haa a high potential to be developed as a characterisation tool for e.g., nanoscale thermal transport, i.e. up to the Brillouin zone boundaries (Figure 6), in semiconductors and nano-devices directly measuring the phonon mean-free-path, demagnetization dynamics of ferromagnets, disentangling the electronic-magnetic-lattice channels, collective dynamics of disordered systems (glasses and liquids), etc. One of the new areas to explore at the nanoscale is that of supercritical fluids, and in particular their non-equilibrium dynamics associated with cluster transitions and density fluctuations in the case of binary mixtures at supercritical conditions, given their importance in several applications.

e) <u>Multidimensional core-level spectroscopies</u>

Finally, the availability of tuneable, As and time-delayed multicolour pulses at HHG and XFEL sources is opening the way towards EUV/X-ray multidimensional spectroscopies that will allow interrogating different atomic centres in a given system directly on the timescale relevant for coherent electronic processes.[308] The full understanding of the entire range of core-level NL methods described above: Stimulated Raman,[171,309] stimulated emission, multiphoton absorption,[136] etc. and the establishment of the element-specificity in TG experiments[195] are

all ingredients for the advent of multidimensional core-level spectroscopies where the cross-talk between different atomic centres, e.g. such as those suspected in 2-centre metal complexes,[310] can be monitored in real-time. The theoretical framework for such experiments has also been developed[245,246,308] and we are confident that these experiments will be realised in the near future.

VI. Conclusions

The above reviewed the state of the art of NL EUV/X-ray methods and presented some of the future scientific questions that could be answered using them. Neither part of the article is supposed to be exhaustive and the future may bring many new developments, especially when combined with technological breakthroughs in terms of light sources, detection schemes, manipulation and control of pulses, etc. Just as for optical domain non-linear optics and spectroscopy in the 1960s, we are witnessing the dawn of a new era in non-linear core-level optics and spectroscopy.

Acknowledgments:

S.M. gratefully acknowledges the support of the Chemical Sciences, Geosciences, and Biosciences division, Office of Basic Energy Sciences, Office of Science, U.S. Department of Energy through Award No. DE-FG02-04ER15571 and of the National Science Foundation (Grant No. -CHE-2246379). MC thanks the Swiss NSF NCCR:MUST and the ERC Advanced Grant DYNAMOX for support. All authors are deeply grateful to their former students and postdocs and to their collaborators for making this work possible.

Table 1 : Comparison of potentially reachable momentum-transfer, spatial-time resolution and selectivity in the Infrared (IR) – optical – Ultraviolet (UV), Extreme Ultraviolet (EUV) soft and hard X-ray Transient Grating spectroscopy. The selectivity column concerns 3d transition metals.

	Energy range	Momentum transfer	Spatial scale	Time scale	Selectivity
IR - Optical - UV	< 5 -10 eV	< 0.02 nm^{-1}	> 125 nm	Down to some fs	Valence shells
EUV	10 – 150 eV	< 0.6 nm^{-1}	> 5 nm	Few fs to as	Mostly M shells
Soft X-ray	150 – 2500 eV	Up to 25 nm^{-1}	> 0.2 nm	fs to as	L, M shells
Hard X-ray	2500 – 20000 eV	Up to 200 nm^{-1}	Down to 0.03 nm	fs to as	K, L, M shells

Figures:

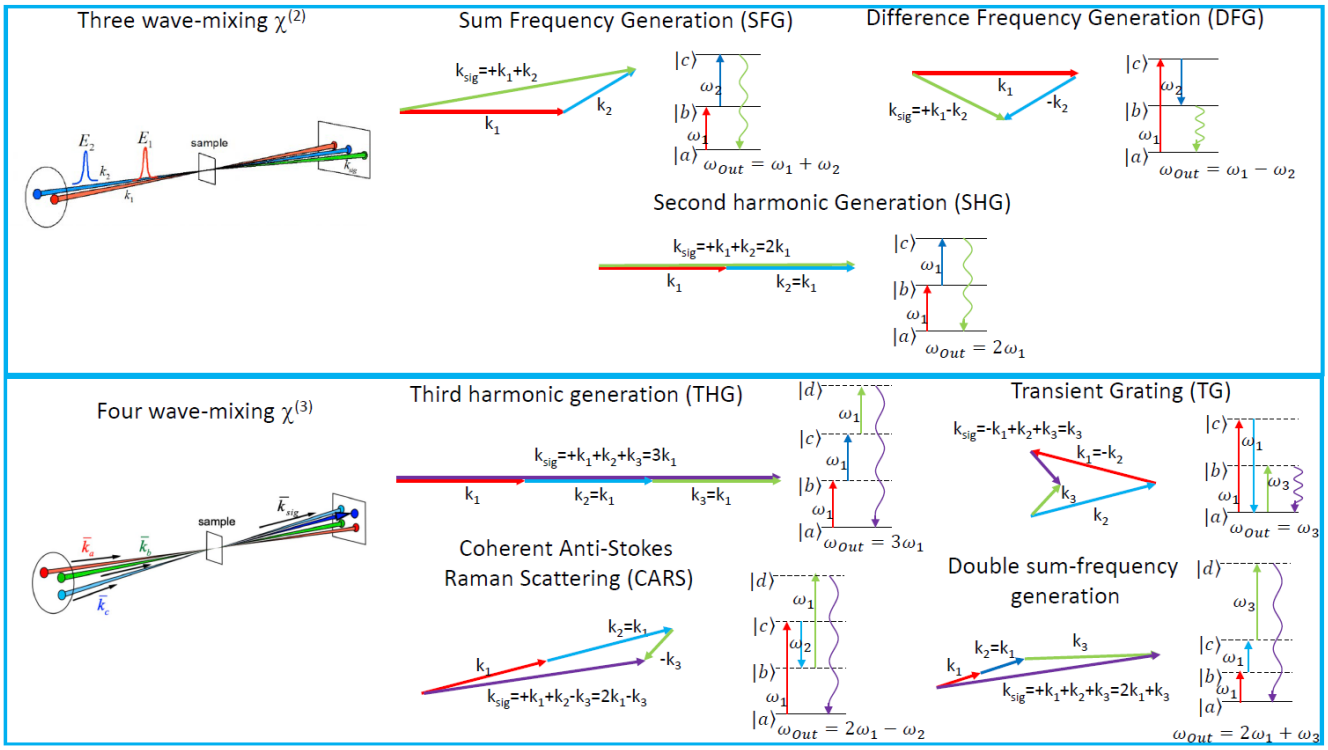

Figure 1: Various example schemes of non-linear optical methods. The upper panel represents some second order processes, while the lower panel shows third order processes. This figure is not exhaustive of all non-linear methods (inspired from ref. [311]).

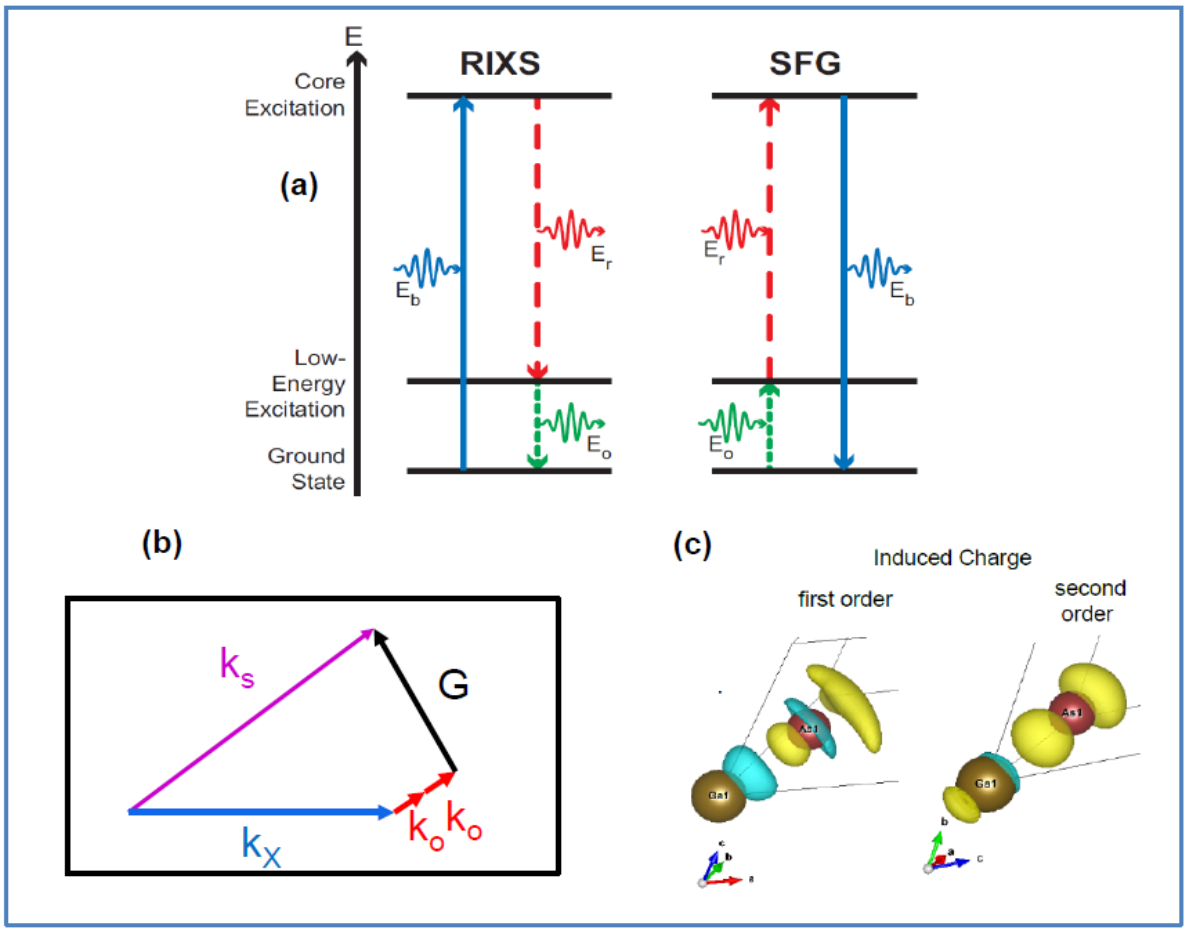

Figure 2: (a) Comparison of the spontaneous and incoherent process of RIXS and the stimulated coherent process of SFG: In a RIXS process, the element-selective core excitation decays spontaneously into a low-energy excitation. The nearly isotropically emitted photons need to be energy-resolved in order to determine the energy loss. In SFG instead, the coherent interaction of the optical and X-ray beams couples the low-energy excitation with the core-excitation. The SFG photon is emitted into the background-free phase matching direction and it does not require to be energy-resolved. In order to map out the low-energy excitation spectrum for a given core excitation, the optical and X-ray photon energies both need to be scanned synchronously. (b) Phase-matching diagram for the second-order optical/X-ray mixing process. (c) Calculated[266] induced first (left) and second order (right) amplitudes of the charge density oscillations in GaAs for an optical field polarized along the (111) direction. Yellow indicates the electron density and blue indicates the hole density. (Reproduced from ref. [266])

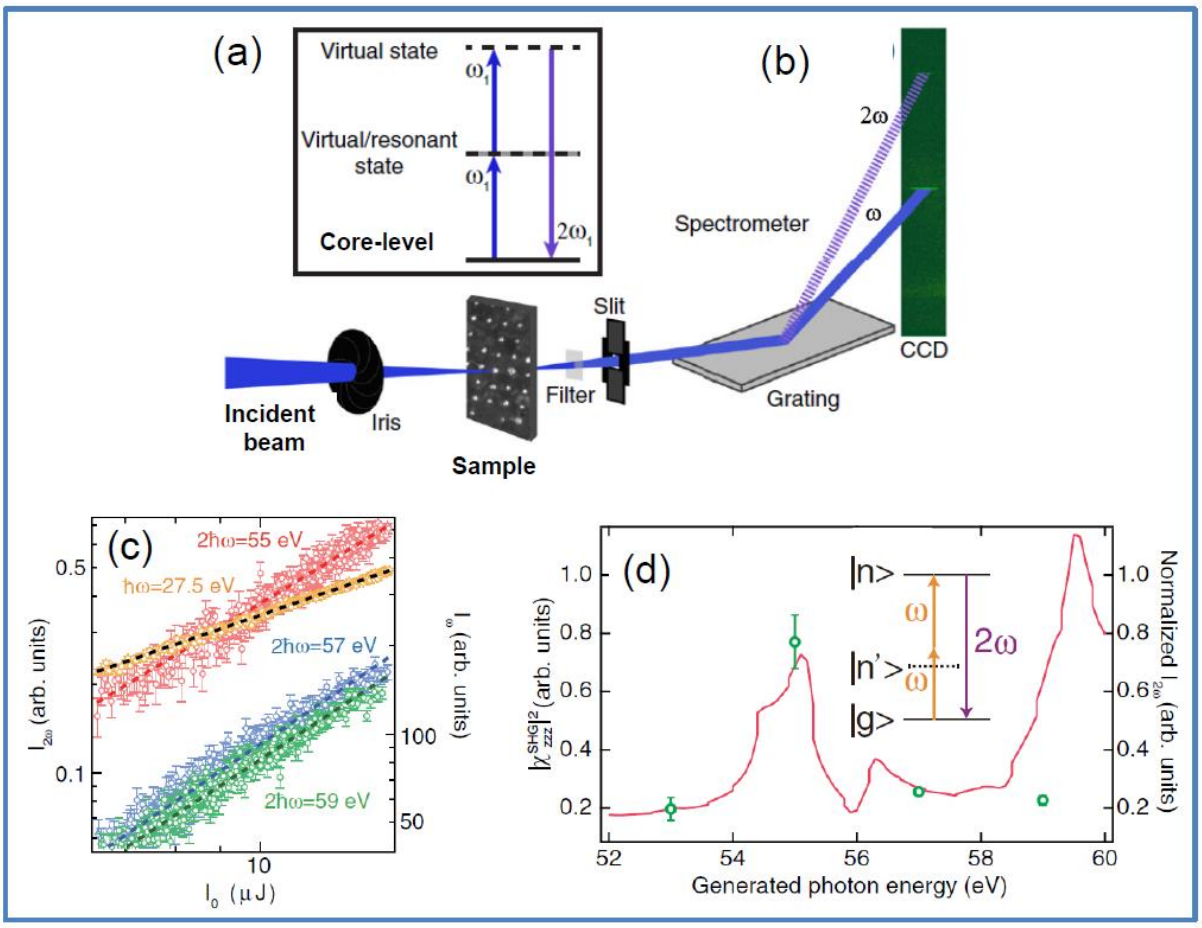

Figure 3: (a) Generic energy level scheme for EUV/X-ray SHG; (b) Configuration for the SHG experiments: The incident beam is focused onto the sample. The transmitted beam and the collinear SH signal (double the fundamental photon energy) are dispersed by a grating, spatially separating the SH signal from the fundamental, which are imaged onto a CCD camera. A reflection geometry (rather than transmission through the sample as shown) has also been used;[184] (c) Quadratic dependence of the $I_{2\omega}$ signals in the case of EUV SHG on a $GaFeO_3$ crystal. $I_{2\omega}$ is plotted on the left axis for the photon energy of $2\hbar\omega$ = 55 eV (red circle), $2\hbar\omega$=57 eV (blue circle), and $2\hbar\omega$ = 59 eV (green circle) in the logarithmic scale. I_{ω} (orange circle) is plotted on the right axis for $\hbar\omega$=27.5 eV. The dashed lines were fitted using a power law (Reproduced from ref. [184]). (d) The SHG signals (green data points) are enhanced by the double resonant effect met by the transition between O 2s → Fe 3d and between the Fe 3p → O 2s state. In the SHG spectrum near the Fe 3p edge for $GaFeO_3$, there are contributions from the inner-shell double resonance at the 3p-edge position and inter-band transitions that give a tail structure in the post-edge region. The red trace represents the calculated $\left|\chi_{zzz}^{SHG}\right|^2$values (left axis) for the energy scheme shown in the inset and the measured ones (right) (green circles) for I_0= 10 μJ, that are normalized by $I_{2\omega}$ at 53 eV.

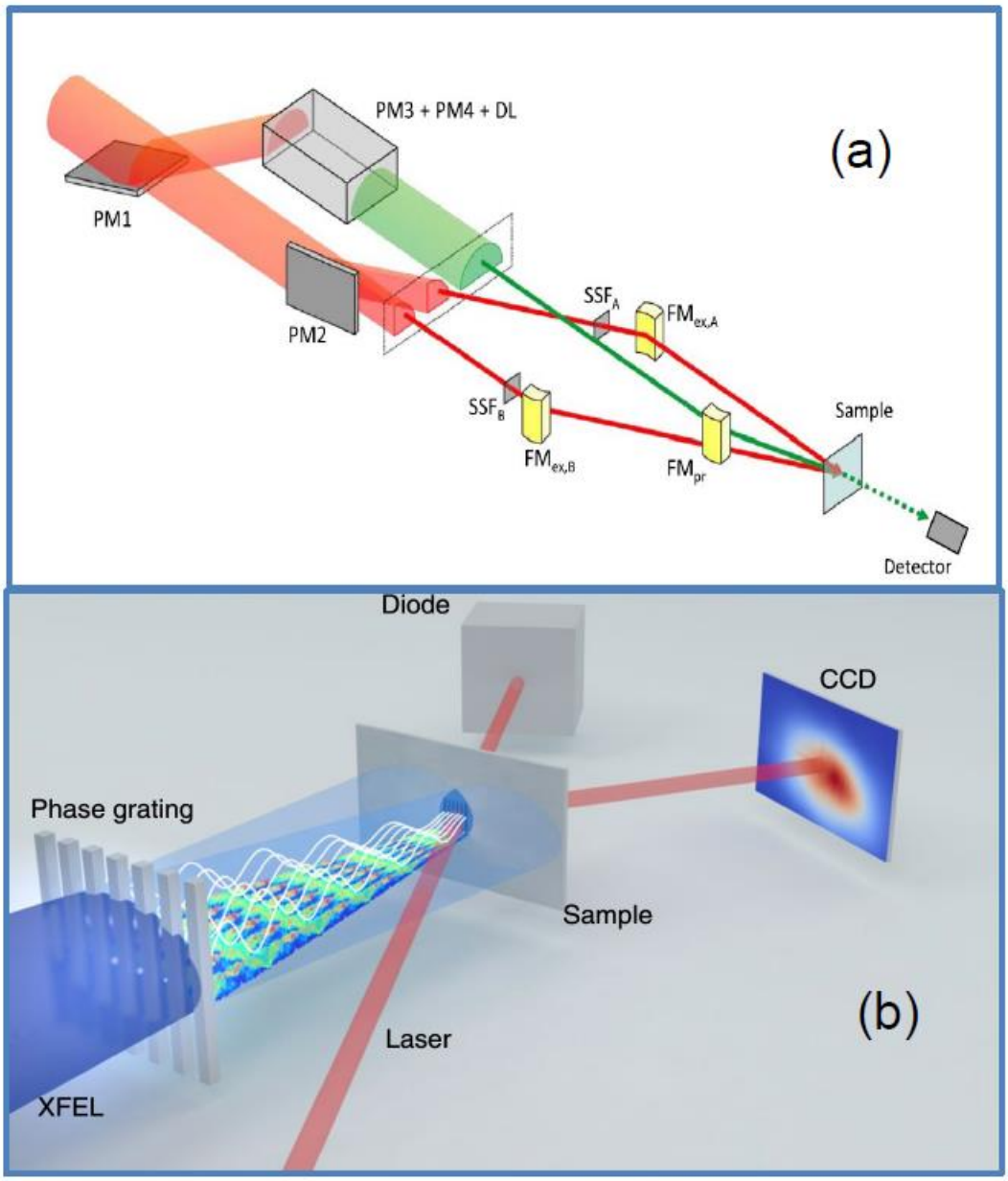

Figure 4: (a) Principle of the split-and-delay scheme used for the all-EUV TG experiment (rep. from ref. [195]); (b) Scheme, based on the Talbot effect, used for the hard X-ray TG probed by an optical pulses (rep. from ref. [202,203])

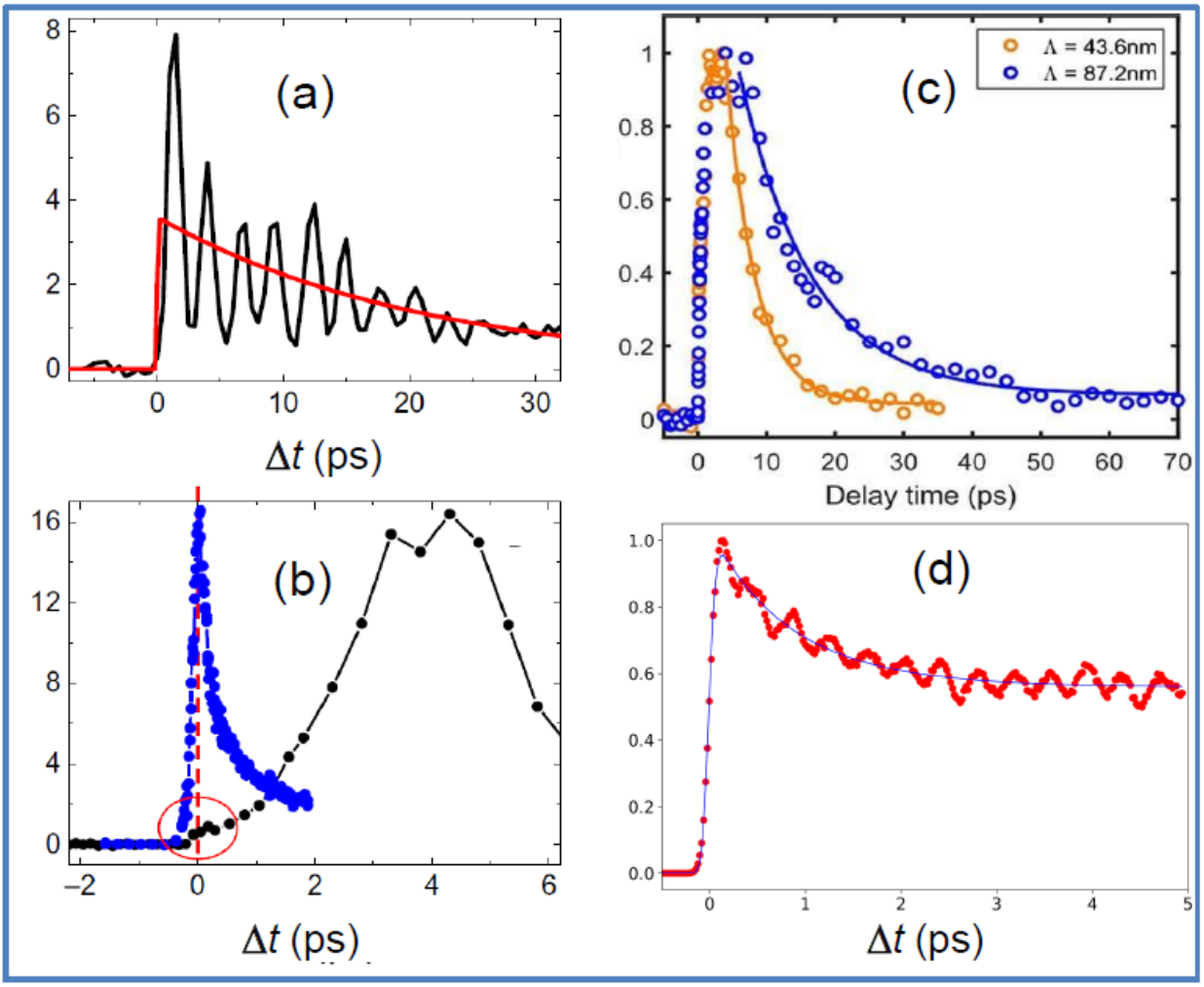

Figure 5: (a) All-EUV TG ($\lambda_{exc}=\lambda_{Probe}$=13.3 nm) signal intensity of Si_3N_4 as a function of Δt for L_{TG}=28 nm. At t<0, the signal is absent because there is no grating in the sample to diffract the probe beam. The signal appears after Δt = 0 and exhibits a slowly decaying component with modulations, matching the frequency of the longitudinal acoustic waves at the wavelength L_{TG}. The slow decaying component (red trace) can be ascribed to a "thermal grating," produced by thermal expansion, modulated by the coherent phonon dynamics and decaying via thermal transport.[196,312] (b) Zoom into the early time response (black dots) and comparison with the EUV TG signal probed by optical pulses (blue dots), where the rise time of the signal is within the cross-correlation. [193,196] The much slower rise of the all-EUV TG signal depends on L_{TG}. The maximum signal is delayed by one-half of the acoustic oscillations period, indicating that the dominant contribution to the signal originates from density changes. Both the slow signal decay (red lines in (a)) and the apparent decay of the oscillations are related to the thermal equilibration time. (c) L_{TG}-dependence (43.6 nm and 87.2 nm) of the all-EUV TG magnetization signal of a 9 nm-thick film of $Co_{0.81}Gd_{0.19}$ deposited on a silicon nitride membrane and probed at the $M_{2,3}$ edge of Co (59.6 eV/20.8 nm). In both cases, the external magnetic field was H = 40 mT. Solid lines are exponential fits with an offset correction (From ref. [200]). (d) hard X-ray signal of bismuth germanate at 7.1 keV (L_{TG}= 770 nm) and probed at 400 nm. Coherent optical phonon oscillations riding on an exponentially decaying signal (fitted by the blue line) can be seen (see text for details).

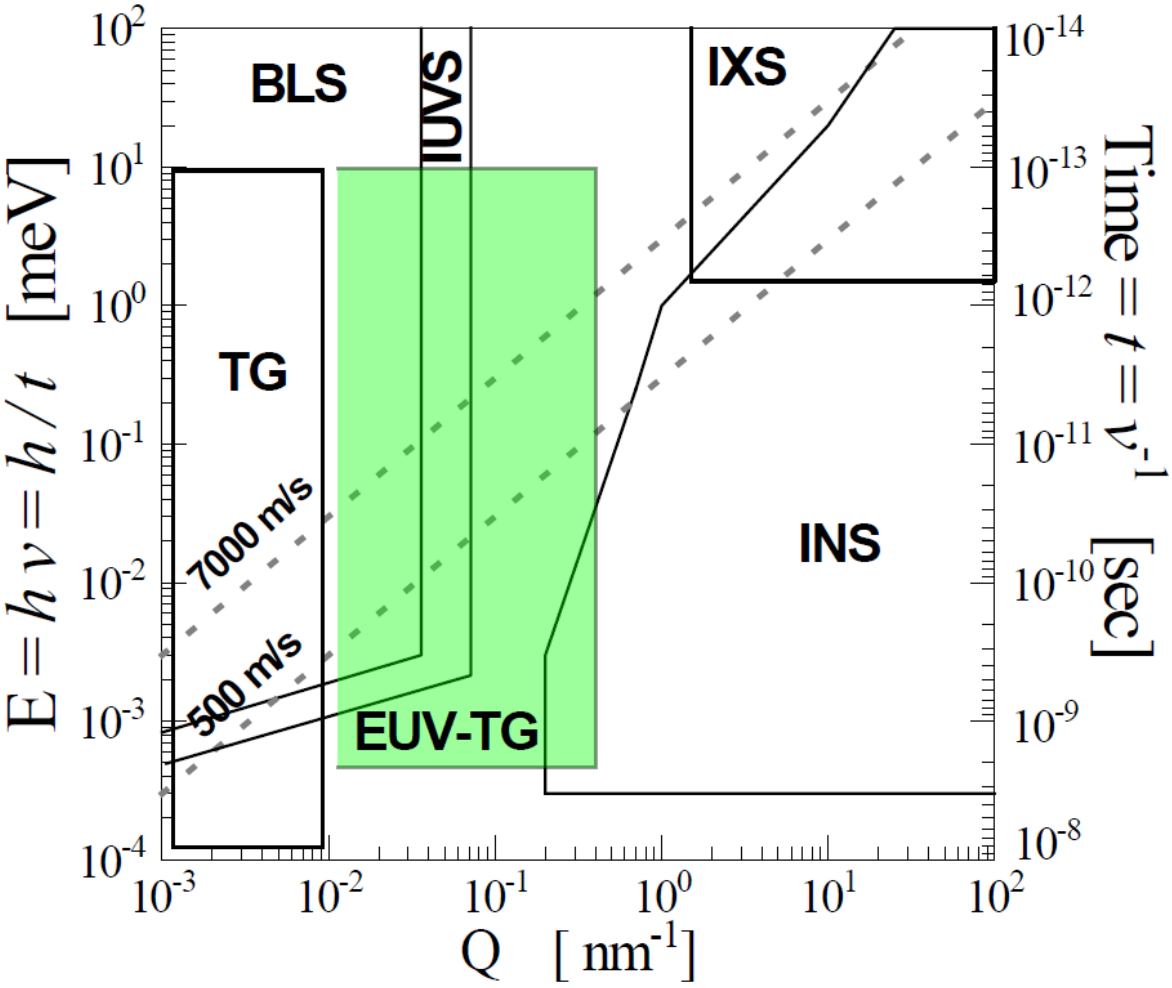

Figure 6: Kinematic regions accessible by existing techniques: Transient Grating (TG), Brillouin Light Scattering (BLS), Inelastic UV Scattering (IUVS), Inelastic X-ray Scattering (IXS) and Inelastic Neutron Scattering (INS). The figure shows the region that is accessible by EUV-TG. The two dotted lines indicate energies of collective excitations with characteristic speeds of sound of 500 m/s and 7000 m/s. Reproduced from ref. [313].

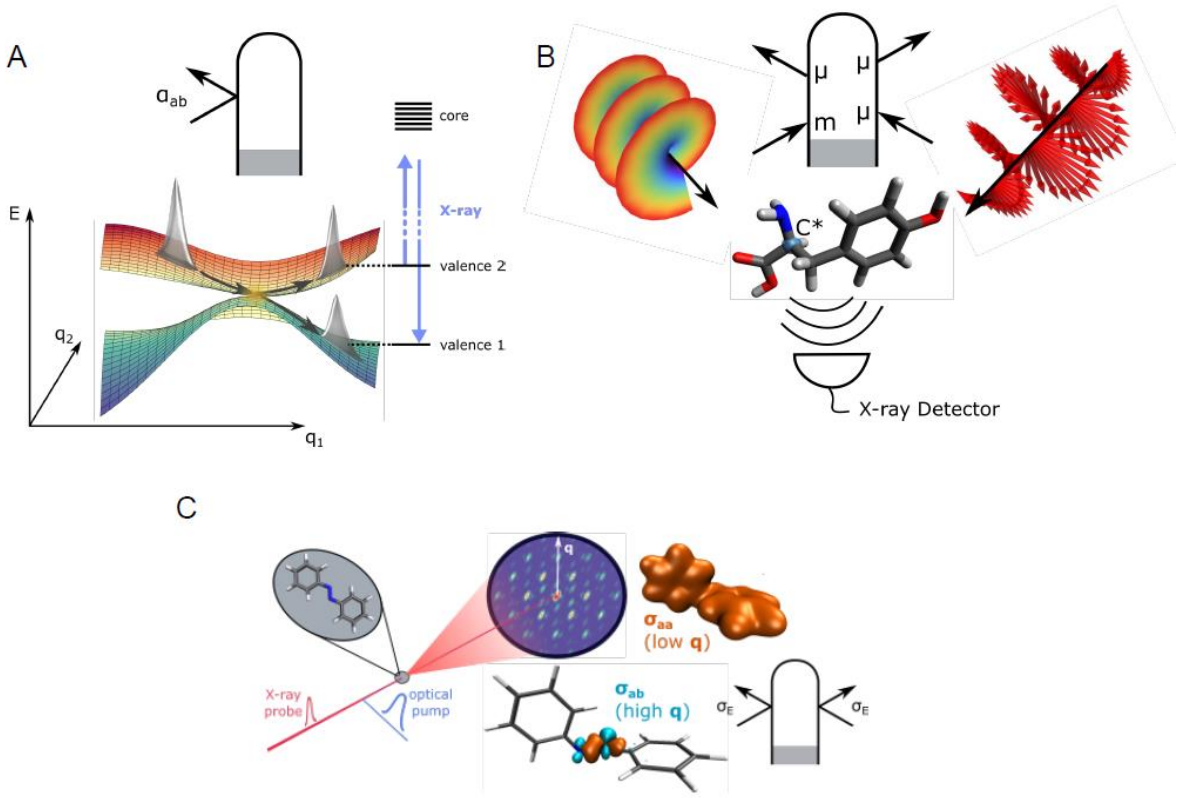

Figure 7: Sketch of theoretically proposed X-ray signals to probe elementary molecular phenomena. (A) Wave packet bifurcation at a conical intersection. In TRUECARS, an off-resonant X-ray field directly probes the emerging coherence via the transition polarizability alpha. (B) X-ray light fields with sophisticated polarization structures probe the chirality of a molecule with a stereogenic centre via dipole moments mu and magnetic moments m. (C) An ultrabright X-ray probe field generates momentum (q-) dependent diffraction patterns of molecular dynamics. Scattering off state densities (all electrons) dominate at low momentum transfer, while scattering off transition densities (one electron) to detect coherences become stronger at high momentum transfer.

1. Kaiser, W. & Garrett, C. G. B. Two-Photon Excitation in Ca${\mathrm{F}}_{2}$: ${\mathrm{Eu}}^{2+}$. *Phys. Rev. Lett.* **7**, 229–231 (1961).

2. Franken, P. A., Hill, A. E., Peters, C. W. & Weinreich, G. Generation of Optical Harmonics. *Phys. Rev. Lett.* **7**, 118–119 (1961).

3. Bloembergen, N. Nonlinear optics and spectroscopy. *Rev. Mod. Phys.* **54**, 685–695 (1982).

4. Mukamel, S. *Principles of nonlinear optical spectroscopy*. (Oxford University Press, 1995).

5. *Principles and Applications of Nonlinear Optical Materials*. (Springer Netherlands, 1993). doi:10.1007/978-94-011-2158-3.

6. Busch, G. E., Jones, R. P. & Rentzepis, P. M. Picosecond spectroscopy using a picosecond continuum. *Chem. Phys. Lett.* **18**, 178–185 (1973).

7. Eisenthal, K. B. Picosecond Relaxation Processes in Chemistry. in *Ultrashort Light Pulses: Picosecond Techniques and Applications* (ed. Shapiro, S. L.) 275–315 (Springer, 1977). doi:10.1007/978-3-662-22574-5_6.

8. Shank, C., Ippen, E. & Bersohn, R. Time-resolved spectroscopy of hemoglobin and its complexes with subpicosecond optical pulses. *Science* **193**, 50 (1976).

9. Zewail, A. H. Femtochemistry: Atomic-Scale Dynamics of the Chemical Bond Using Ultrafast Lasers (Nobel Lecture). *Angew. Chem. Int. Ed.* **39**, 2586–2631 (2000).

10. Ackermann, W. *et al.* Operation of a free-electron laser from the extreme ultraviolet to the water window. *Nat. Photonics* **1**, 336–342 (2007).

11. Allaria, E. *et al.* The FERMI@ Elettra free-electron-laser source for coherent x-ray physics: photon properties, beam transport system and applications. *New J. Phys.* **12**, 075002 (2010).

12. Emma, P. *et al.* First lasing and operation of an angstrom-wavelength free-electron laser. *Nat. Photonics* **4**, 641–647 (2010).

13. Ishikawa, T. *et al.* A compact X-ray free-electron laser emitting in the sub-angstrom region. *Nat. Photonics* **6**, 540–544 (2012).

14. Prat, E. *et al.* A compact and cost-effective hard X-ray free-electron laser driven by a high-brightness and low-energy electron beam. *Nat. Photonics* **14**, 748–754 (2020).

15. Lappas, D. G. & L'Huillier, A. Generation of attosecond xuv pulses in strong laser-atom interactions. *Phys. Rev. A* **58**, 4140–4146 (1998).

16. Corkum, P. B., Burnett, N. H. & Ivanov, M. Y. Subfemtosecond Pulses. *Opt. Lett.* **19**, 1870–1872 (1994).

17. Drescher, M. *et al.* X-ray pulses approaching the attosecond frontier. *Science* **291**, 1923–1927 (2001).

18. Christov, I. P., Murnane, M. M. & Kapteyn, H. C. High-harmonic generation of attosecond pulses in the '"single-cycle"' regime. *Phys. Rev. Lett.* **78**, 1251–1254 (1997).

19. Chang, Z. H., Rundquist, A., Wang, H. W., Murnane, M. M. & Kapteyn, H. C. Generation of coherent soft X rays at 2.7 nm using high harmonics. *Phys. Rev. Lett.* **79**, 2967–2970 (1997).

20. Hentschel, M. *et al.* Attosecond metrology. *Nature* **414**, 509–513 (2001).

21. Lenzner, M., Schnurer, M., Spielmann, C. & Krausz, F. Extreme nonlinear optics with few-cycle laser pulses. *Ieice Trans. Electron.* **E81C**, 112–122 (1998).

22. Milne, C. J., Penfold, T. J. & Chergui, M. Recent experimental and theoretical developments in time-resolved X-ray spectroscopies. *Coord. Chem. Rev.* **277**, 44–68 (2014).

23. Chergui, M. & Collet, E. Photoinduced Structural Dynamics of Molecular Systems Mapped by Time-Resolved X-ray Methods. *Chem. Rev.* **117**, 11025–11065 (2017).

24. Kraus, P. M., Zürch, M., Cushing, S. K., Neumark, D. M. & Leone, S. R. The ultrafast X-ray spectroscopic revolution in chemical dynamics. *Nat. Rev. Chem.* **2**, 82–94 (2018).

25. Zong, A., Nebgen, B. R., Lin, S.-C., Spies, J. A. & Zuerch, M. Emerging ultrafast techniques for studying quantum materials. *Nat. Rev. Mater.* 1–17 (2023) doi:10.1038/s41578-022-00530-0.

26. Rohringer, N. X-ray Raman scattering: a building block for nonlinear spectroscopy. *Philos. Trans. R. Soc. Math. Phys. Eng. Sci.* **377**, 20170471 (2019).

27. Leone, S. R. & Neumark, D. M. Probing matter with nonlinear spectroscopy. *Science* **379**, 536–537 (2023).

28. Khan, S. Free-electron lasers. *J. Mod. Opt.* **55**, 3469–3512 (2008).

29. Schoenlein, R. *et al.* Recent advances in ultrafast X-ray sources. *Philos. Trans. R. Soc. Math. Phys. Eng. Sci.* **377**, 20180384 (2019).

30. Biegert, J., Calegari, F., Dudovich, N., Quéré, F. & Vrakking, M. Attosecond technology(ies) and science. *J. Phys. B At. Mol. Opt. Phys.* **54**, 070201 (2021).

31. Huang, N., Deng, H., Liu, B., Wang, D. & Zhao, Z. Features and futures of X-ray free-electron lasers. *The Innovation* **2**, 100097 (2021).

32. Pellegrini, C., Marinelli, A. & Reiche, S. The physics of x-ray free-electron lasers. *Rev. Mod. Phys.* **88**, 015006 (2016).

33. Margaritondo, G. & Rafelski, J. The relativistic foundations of synchrotron radiation. *J. Synchrotron Radiat.* **24**, 898–901 (2017).

34. Kondratenko, A. M. & Saldin, E. L. GENERATION OF COHERENT RADIATION BY A RELATIVISTIC ELECTRON BEAM IN AN ONDULATOR. *Part. Accel.* **10**, 207–216 (1980).

35. Allaria, E. *et al.* Highly coherent and stable pulses from the FERMI seeded free-electron laser in the extreme ultraviolet. *Nat. Photonics* **6**, 699–704 (2012).

36. Abela, R. *et al.* Perspective: Opportunities for ultrafast science at SwissFEL. *Struct. Dyn.* **4**, 061602 (2017).

37. Altarelli, M., Brinkmann, R. & Chergui, M. The European X-ray free-electron laser. Technical design report. (2007).

38. Tschentscher, T. *et al.* Photon Beam Transport and Scientific Instruments at the European XFEL. *Appl. Sci.* **7**, 592 (2017).

39. Kang, H.-S. *et al.* Hard X-ray free-electron laser with femtosecond-scale timing jitter. *Nat. Photonics* **11**, 708–713 (2017).

40. Yu, L.-H. *et al.* High-Gain Harmonic-Generation Free-Electron Laser. *Science* **289**, 932–934 (2000).

41. Allaria, E. *et al.* Two-stage seeded soft-X-ray free-electron laser. *Nat. Photonics* **7**, 913–918 (2013).

42. Rebernik Ribič, P. *et al.* Coherent soft X-ray pulses from an echo-enabled harmonic generation free-electron laser. *Nat. Photonics* **13**, 555–561 (2019).

43. Gianessi, L. & Masciovecchio, C. *FERMI 2.0 Conceptual design report*. https://www.elettra.eu/images/Documents/FERMI%20Machine/Machine/CDR/FERMI2.0CDR.pdf (2022).

44. FLASH Upgrades. https://flash.desy.de/flash_upgrades/.

45. McPherson, A. *et al.* Studies of multiphoton production of vacuum-ultraviolet radiation in the rare gases. *JOSA B* **4**, 595–601 (1987).

46. Ferray, M. *et al.* Multiple-harmonic conversion of 1064 nm radiation in rare gases. *J. Phys. B At. Mol. Opt. Phys.* **21**, L31–L35 (1988).

47. Corkum, P. B. & Krausz, F. Attosecond science. *Nat. Phys.* **3**, 381–387 (2007).

48. DiChiara, A. D. *et al.* Scaling of High-Order Harmonic Generation in the Long Wavelength Limit of a Strong Laser Field. *IEEE J. Sel. Top. Quantum Electron.* **18**, 419–433 (2012).

49. Cousin, S. L. *et al.* High-flux table-top soft x-ray source driven by sub-2-cycle, CEP stable, 1.85-mu m 1-kHz pulses for carbon K-edge spectroscopy. *Opt. Lett.* **39**, 5383–5386 (2014).

50. Kleine, C. *et al.* Soft X-ray Absorption Spectroscopy of Aqueous Solutions Using a Table-Top Femtosecond Soft X-ray Source. *J. Phys. Chem. Lett.* **10**, 52–58 (2019).

51. Chang, Z. Enhancing keV high harmonic signals generated by long-wave infrared lasers. *OSA Contin.* **2**, 2131–2136 (2019).

52. Kroh, T. *et al.* Enhanced high-harmonic generation up to the soft X-ray region driven by mid-infrared pulses mixed with their third harmonic. *Opt. Express* **26**, 16955–16969 (2018).

53. Makos, I. *et al.* A 10-gigawatt attosecond source for non-linear XUV optics and XUV-pump-XUV-probe studies. *Sci. Rep.* **10**, 3759 (2020).

54. Pupeza, I. *et al.* Compact high-repetition-rate source of coherent 100 eV radiation. *Nat. Photonics* **7**, 608–612 (2013).

55. Hädrich, S. *et al.* Exploring new avenues in high repetition rate table-top coherent extreme ultraviolet sources. *Light Sci. Appl.* **4**, e320–e320 (2015).

56. Rossi, G. M. *et al.* Sub-cycle millijoule-level parametric waveform synthesizer for attosecond science. *Nat. Photonics* **14**, 629–635 (2020).

57. Geneaux, R., Marroux, H. J. B., Guggenmos, A., Neumark, D. M. & Leone, S. R. Transient absorption spectroscopy using high harmonic generation: a review of ultrafast X-ray dynamics in molecules and solids. *Philos. Trans. R. Soc. Math. Phys. Eng. Sci.* **377**, 20170463 (2019).

58. Park, J., Subramani, A., Kim, S. & Ciappina, M. F. Recent trends in high-order harmonic generation in solids. *Adv. Phys. X* **7**, 2003244 (2022).

59. Luu, T. T. *et al.* Extreme–ultraviolet high–harmonic generation in liquids. *Nat. Commun.* **9**, 3723 (2018).

60. Zeng, A.-W. & Bian, X.-B. Impact of Statistical Fluctuations on High Harmonic Generation in Liquids. *Phys. Rev. Lett.* **124**, 203901 (2020).

61. Agostini, P. & DiMauro, L. F. The physics of attosecond light pulses. *Rep. Prog. Phys.* **67**, 813–855 (2004).

62. Gallmann, L., Cirelli, C. & Keller, U. Attosecond science: recent highlights and future trends. *Annu. Rev. Phys. Chem.* **63**, 447–469 (2012).

63. Krausz, F. & Ivanov, M. Attosecond physics. *Rev. Mod. Phys.* **81**, 163 (2009).

64. Frank, F. *et al.* Invited Review Article: Technology for Attosecond Science. *Rev. Sci. Instrum.* **83**, 071101 (2012).

65. Boutu, W., Ducousso, M., Hergott, J.-F. & Merdji, H. Overview on HHG High-Flux Sources. in *Optical Technologies for Extreme-Ultraviolet and Soft X-ray Coherent Sources* (eds. Canova, F. & Poletto, L.) 63–78 (Springer, 2015). doi:10.1007/978-3-662-47443-3_4.

66. Franz, D. *et al.* All semiconductor enhanced high-harmonic generation from a single nanostructured cone. *Sci. Rep.* **9**, 5663 (2019).

67. Jürgens, P. *et al.* Origin of strong-field-induced low-order harmonic generation in amorphous quartz. *Nat. Phys.* **16**, 1035–1039 (2020).

68. Gholam-Mirzaei, S., Beetar, J. E., Chacón, A. & Chini, M. High-harmonic generation in ZnO driven by self-compressed mid-infrared pulses. *JOSA B* **35**, A27–A31 (2018).

69. Pertot, Y. *et al.* Time-resolved x-ray absorption spectroscopy with a water window high-harmonic source. *Science* **355**, 264–267 (2017).

70. Zinchenko, K. S. *et al.* Sub-7-femtosecond conical-intersection dynamics probed at the carbon K-edge. *Science* **371**, 489–494 (2021).

71. Gallmann, L. *et al.* Photoemission and photoionization time delays and rates. *Struct. Dyn.* **4**, (2017).

72. Faccialà, D. *et al.* Time-resolved chiral X-Ray photoelectron spectroscopy with transiently enhanced atomic site-selectivity: a Free Electron Laser investigation of

electronically excited fenchone enantiomers. Preprint at https://doi.org/10.48550/arXiv.2202.13704 (2022).

73. Wörner, H. J., Bertrand, J. B., Kartashov, D. V., Corkum, P. B. & Villeneuve, D. M. Following a chemical reaction using high-harmonic interferometry. *Nature* **466**, 604–607 (2010).

74. Abel, B., Buck, U., Sobolewski, A. L. & Domcke, W. On the nature and signatures of the solvated electron in water. *Phys. Chem. Chem. Phys.* **14**, 22–34 (2012).

75. Hummert, J. *et al.* Femtosecond Extreme Ultraviolet Photoelectron Spectroscopy of Organic Molecules in Aqueous Solution. *J. Phys. Chem. Lett.* **9**, 6649–6655 (2018).

76. Longetti, L. *et al.* Ultrafast photoelectron spectroscopy of photoexcited aqueous ferrioxalate. *Phys. Chem. Chem. Phys.* **23**, 25308–25316 (2021).

77. Arrell, C. A. *et al.* Laser-Assisted Photoelectric Effect from Liquids. *Phys. Rev. Lett.* **117**, (2016).

78. Crepaldi, A. *et al.* Time-resolved ARPES at LACUS: Band Structure and Ultrafast Electron Dynamics of Solids. *Chimia* **71**, 273–277 (2017).

79. Gatti, G. *et al.* Light-Induced Renormalization of the Dirac Quasiparticles in the Nodal-Line Semimetal ZrSiSe. *Phys. Rev. Lett.* **125**, 076401 (2020).

80. Fidler, A. P. *et al.* Nonlinear XUV signal generation probed by transient grating spectroscopy with attosecond pulses. *Nat. Commun.* **10**, 1384 (2019).

81. Grilj, J. *et al.* Self Referencing Heterodyne Transient Grating Spectroscopy with Short Wavelength. *Photonics* **2**, 392–401 (2015).

82. Cao, W., Warrick, E. R., Fidler, A., Neumark, D. M. & Leone, S. R. Noncollinear wave mixing of attosecond XUV and few-cycle optical laser pulses in gas-phase atoms: Toward multidimensional spectroscopy involving XUV excitations. *Phys. Rev. A* **94**, 053846 (2016).

83. Mairesse, Y. *et al.* High-Order Harmonic Transient Grating Spectroscopy in a Molecular Jet. *Phys. Rev. Lett.* **100**, 143903 (2008).

84. Ruf, H. *et al.* High-harmonic transient grating spectroscopy of NO_2 electronic relaxation. *J. Chem. Phys.* **137**, 224303 (2012).

85. Orfanos, I. *et al.* Non-linear processes in the extreme ultraviolet. *J. Phys. Photonics* **2**, 042003 (2020).

86. Senfftleben, B. *et al.* Highly non-linear ionization of atoms induced by intense high-harmonic pulses. *J. Phys. Photonics* **2**, 034001 (2020).

87. Drescher, L. *et al.* Extreme-ultraviolet spectral compression by four-wave mixing. *Nat. Photonics* 1–4 (2021) doi:10.1038/s41566-020-00758-8.

88. Helk, T. *et al.* Table-top extreme ultraviolet second harmonic generation. *Sci. Adv.* **7**, eabe2265.

89. Shen, Y. R. Principles of nonlinear optics. (1984).

90. Boyd, R. W. *Nonlinear Optics*. (Academic Press, 2020).

91. Corn, R. M. & Higgins, D. A. Optical second harmonic generation as a probe of surface chemistry. *Chem. Rev.* **94**, 107–125 (1994).

92. Shi, X., Borguet, E., Tarnovsky, A. N. & Eisenthal, K. B. Ultrafast dynamics and structure at aqueous interfaces by second harmonic generation. *Chem. Phys.* **205**, 167–178 (1996).

93. Wang, H., Borguet, E. & Eisenthal, K. B. Polarity of Liquid Interfaces by Second Harmonic Generation Spectroscopy. *J. Phys. Chem. A* **101**, 713–718 (1997).

94. Eisenthal, K. B. Liquid Interfaces Probed by Second-Harmonic and Sum-Frequency Spectroscopy. *Chem. Rev.* **96**, 1343–1360 (1996).

95. Almogy, G. & Yariv, A. Resonantly-enhanced nonlinear optics of intersubband transitions. *J. Nonlinear Opt. Phys. Mater.* **04**, 401–458 (1995).

96. Oudar, J.-L. & Shen, Y. R. Nonlinear spectroscopy by multiresonant four-wave mixing. *Phys. Rev. A* **22**, 1141–1158 (1980).

97. Begley, R. F., Harvey, A. B. & Byer, R. L. Coherent anti-Stokes Raman spectroscopy. *Appl. Phys. Lett.* **25**, 387–390 (1974).

98. Giordmaine, J. A. Mixing of Light Beams in Crystals. *Phys. Rev. Lett.* **8**, 19–20 (1962).

99. Jones, W. J. & Stoicheff, B. P. Inverse Raman Spectra: Induced Absorption at Optical Frequencies. *Phys. Rev. Lett.* **13**, 657–659 (1964).

100. Maker, P. D. & Terhune, R. W. Study of Optical Effects Due to an Induced Polarization Third Order in the Electric Field Strength. *Phys. Rev.* **137**, A801–A818 (1965).

101. Duncan, M. D., Reintjes, J. & Manuccia, T. J. Scanning coherent anti-Stokes Raman microscope. *Opt. Lett.* **7**, 350–352 (1982).

102. Hofmann, F., Short, M. P. & Dennett, C. A. Transient grating spectroscopy: An ultrarapid, nondestructive materials evaluation technique. *MRS Bull.* **44**, 392–402 (2019).

103. Ernst, R. R., Bodenhausen, G. & Wokaun, A. *Principles of nuclear magnetic resonance in one and two dimensions*. vol. 14 (Clarendon Press Oxford, 1987).

104. Mukamel, S., Tanimura, Y. & Hamm, P. Coherent Multidimensional Optical Spectroscopy. *Acc. Chem. Res.* **42**, 1207–1209 (2009).

105. Hamm, P. & Zanni, M. *Concepts and methods of 2d infrared spectroscopy*. (Cambridge University Press).

106. Brixner, T., Stiopkin, I. V. & Fleming, G. R. Tunable two-dimensional femtosecond spectroscopy. *Opt. Lett.* **29**, 884–886 (2004).

107. Brixner, T. *et al.* Two-dimensional spectroscopy of electronic couplings in photosynthesis. *Nature* **434**, 625–628 (2005).

108. Haddad, A. A. *et al.* Set-up for broadband Fourier-transform multidimensional electronic spectroscopy. *Opt. Lett.* **40**, 312–315 (2015).

109. Auböck, G., Consani, C., Mourik, F. van & Chergui, M. Ultrabroadband femtosecond two-dimensional ultraviolet transient absorption. *Opt. Lett.* **37**, 2337–2339 (2012).

110. Consani, C., Aubock, G., van Mourik, F. & Chergui, M. Ultrafast Tryptophan-to-Haem Electron Transfer in Myoglobins revealed by UV 2D spectroscopy. *Science* **339**, 1586–1589 (2013).

111. Borrego-Varillas, R. *et al.* Two-dimensional electronic spectroscopy in the ultraviolet by a birefringent delay line. *Opt. Express* **24**, 28491–28499 (2016).

112. Freund, I. & Levine, B. F. Parametric Conversion of X Rays. *Phys. Rev. Lett.* **23**, 854–857 (1969).

113. Eisenberger, P. & McCall, S. L. X-Ray Parametric Conversion. *Phys. Rev. Lett.* **26**, 684–688 (1971).

114. Eisenberger, P. M. & McCall, S. L. Mixing of X-Ray and Optical Photons. *Phys. Rev. A* **3**, 1145–1151 (1971).

115. Woo, J. W. F. & Jha, S. S. Inelastic Scattering of X Rays from Optically Induced Charge-Density Oscillations. *Phys. Rev. B* **6**, 4081–4082 (1972).

116. Freund, I. Nonlinear X-ray spectroscopy. *Opt. Commun.* **6**, 421–423 (1972).

117. Freund, I. & Levine, B. F. Surface Effects in the Nonlinear Interaction of X-Ray and Optical Fields. *Phys. Rev. B* **8**, 3059–3060 (1973).

118. Flytzanis, C. DETERMINATION OF LOCAL FIELD IN DIELECTRIC. *COMPTES RENDUS HEBDOMADAIRES DES SEANCES DE L ACADEMIE DES SCIENCES, SERIE B* 339–342 (1975).

119. Danino, H. & Freund, I. Parametric Down Conversion of X Rays into the Extreme Ultraviolet. *Phys. Rev. Lett.* **46**, 1127–1130 (1981).

120. Tanaka, S., Chernyak, V. & Mukamel, S. Time-resolved x-ray spectroscopies: Nonlinear response functions and Liouville-space pathways. *Phys. Rev. A* **63**, 063405 (2001).

121. Tanaka, S. & Mukamel, S. Coherent X-Ray Raman Spectroscopy: A Nonlinear Local Probe for Electronic Excitations. *Phys. Rev. Lett.* **89**, 043001 (2002).

122. Tanaka, S. & Mukamel, S. X-ray four-wave mixing in molecules. *J. Chem. Phys.* **116**, 1877–1891 (2002).

123. Doumy, G. *et al.* Nonlinear Atomic Response to Intense Ultrashort X Rays. *Phys. Rev. Lett.* **106**, 083002 (2011).

124. Serrat, C. Localized Core Four-Wave Mixing Buildup in the X-ray Spectrum of Chemical Species. *J. Phys. Chem. Lett.* 1093–1097 (2021) doi:10.1021/acs.jpclett.0c03270.

125. Serrat, C. Resonantly Enhanced Difference-Frequency Generation in the Core X-ray Absorption of Molecules. *J. Phys. Chem. A* **125**, 10706–10710 (2021).

126. Haber, J. *et al.* Nonlinear resonant X-ray Raman scattering. Preprint at https://doi.org/10.48550/arXiv.2006.14724 (2020).

127. Popova-Gorelova, D., Reis, D. A. & Santra, R. Theory of x-ray scattering from laser-driven electronic systems. *Phys. Rev. B* **98**, 224302 (2018).

128. Misoguti, L., Christov, I. P., Backus, S., Murnane, M. M. & Kapteyn, H. C. Nonlinear wave-mixing processes in the extreme ultraviolet. *Phys. Rev. A* **72**, 063803 (2005).

129. Maznev, A. A., Nelson, K. A. & Rogers, J. A. Optical heterodyne detection of laser-induced gratings. *Opt. Lett.* **23**, 1319–1321 (1998).

130. Katayama, K., Yamaguchi, M. & Sawada, T. Lens-free heterodyne detection for transient grating experiments. *Appl. Phys. Lett.* **82**, 2775–2777 (2003).

131. Sorokin, A. A. *et al.* Photoelectric Effect at Ultrahigh Intensities. *Phys. Rev. Lett.* **99**, 213002 (2007).

132. Kanter, E. P. *et al.* Unveiling and Driving Hidden Resonances with High-Fluence, High-Intensity X-Ray Pulses. *Phys. Rev. Lett.* **107**, 233001 (2011).

133. Lambropoulos, P. & Tang, X. Multiple excitation and ionization of atoms by strong lasers. *JOSA B* **4**, 821–832 (1987).

134. Novikov, S. A. & Hopersky, A. N. Two-photon excitation-ionization of the 1s shell of highly charged positive atomic ions. *J. Phys. B At. Mol. Opt. Phys.* **34**, 4857–4863 (2001).

135. Sytcheva, A., Pabst, S., Son, S.-K. & Santra, R. Enhanced nonlinear response of Ne^{8+} to intense ultrafast x rays. *Phys. Rev. A* **85**, 023414 (2012).

136. Tamasaku, K. *et al.* X-ray two-photon absorption competing against single and sequential multiphoton processes. *Nat. Photonics* **8**, 313–316 (2014).

137. Ghimire, S. *et al.* Nonsequential two-photon absorption from the K shell in solid zirconium. *Phys. Rev. A* **94**, 043418 (2016).

138. Tamasaku, K. *et al.* Nonlinear Spectroscopy with X-Ray Two-Photon Absorption in Metallic Copper. *Phys. Rev. Lett.* **121**, 083901 (2018).

139. Powers, P. E. & Haus, J. W. *Fundamentals of Nonlinear Optics*. (CRC Press, 2017). doi:10.1201/9781315116433.

140. Paschotta, R. & Keller, U. Passive mode locking with slow saturable absorbers. *Appl. Phys. B* **73**, 653–662 (2001).

141. Wang, G. *et al.* Broadband saturable absorption and exciton-exciton annihilation in $MoSe_2$ composite thin films. *Opt. Mater. Express* **9**, 483–496 (2019).

142. Kumar, S. *et al.* Femtosecond carrier dynamics and saturable absorption in graphene suspensions. *Appl. Phys. Lett.* **95**, 191911 (2009).

143. Bob Nagler et al. Turning solid aluminium transparent by intense soft X-ray photoionization. *Nat. Phys.* **5**, 693–696 (2009).

144. Yoneda, H. *et al.* Ultra-fast switching of light by absorption saturation in vacuum ultra-violet region. *Opt. Express* **17**, 23443–23448 (2009).

145. Yoneda, H. *et al.* Saturable absorption of intense hard X-rays in iron. *Nat. Commun.* **5**, 5080 (2014).

146. Hoffmann, L. *et al.* Saturable Absorption of Free-Electron Laser Radiation by Graphite near the Carbon K-Edge. *J. Phys. Chem. Lett.* **13**, 8963–8970 (2022).

147. Rohringer, N. *et al.* Atomic inner-shell X-ray laser at 1.46 nanometres pumped by an X-ray free-electron laser. *Nature* **481**, 488–491 (2012).

148. Beye, M. *et al.* Stimulated X-ray emission for materials science. *Nature* **501**, 191–194 (2013).

149. Jonnard, P. *et al.* EUV stimulated emission from MgO pumped by FEL pulses. *Struct. Dyn.* **4**, 054306 (2017).

150. Yoneda, H. *et al.* Atomic inner-shell laser at 1.5-ångström wavelength pumped by an X-ray free-electron laser. *Nature* **524**, 446–449 (2015).

151. Glatzel, P. & Bergmann, U. High resolution 1s core hole X-ray spectroscopy in 3d transition metal complexes - electronic and structural information. *Coord. Chem. Rev.* **249**, 65–95 (2005).

152. Zhang, W. *et al.* Tracking excited-state charge and spin dynamics in iron coordination complexes. *Nature* **509**, 345–348 (2014).

153. Kinschel, D. *et al.* Femtosecond X-ray emission study of the spin cross-over dynamics in haem proteins. *Nat. Commun.* **11**, 4145 (2020).

154. Bacellar, C. *et al.* Spin cascade and doming in ferric hemes: Femtosecond X-ray absorption and X-ray emission studies. *Proc. Natl. Acad. Sci.* **117**, 21914–21920 (2020).

155. March, A. M. *et al.* Probing Transient Valence Orbital Changes with Picosecond Valence-to-Core X-ray Emission Spectroscopy. *J. Phys. Chem. C* **121**, 2620–2626 (2017).

156. Ledbetter, K. *et al.* Excited state charge distribution and bond expansion of ferrous complexes observed with femtosecond valence-to-core x-ray emission spectroscopy. *J. Chem. Phys.* **152**, 074203 (2020).

157. Kroll, T. *et al.* Stimulated X-Ray Emission Spectroscopy in Transition Metal Complexes. *Phys. Rev. Lett.* **120**, 133203 (2018).

158. Duris, J. *et al.* Tunable isolated attosecond X-ray pulses with gigawatt peak power from a free-electron laser. *Nat. Photonics* **14**, 30–36 (2020).

159. McCamant, D. W., Kukura, P. & Mathies, R. A. Femtosecond stimulated Raman study of excited-state evolution in bacteriorhodopsin. *J. Phys. Chem. B* **109**, 10449–10457 (2005).

160. Kukura, P., McCamant, D. W. & Mathies, R. A. Femtosecond Stimulated Raman Spectroscopy. *Annu. Rev. Phys. Chem.* **58**, 461–488 (2007).

161. Hahn, A. W. *et al.* Probing the Valence Electronic Structure of Low-Spin Ferrous and Ferric Complexes Using 2p3d Resonant Inelastic X-ray Scattering (RIXS). *Inorg. Chem.* **57**, 9515–9530 (2018).

162. Van Kuiken, B. E. *et al.* Electronic Spectra of Iron–Sulfur Complexes Measured by 2p3d RIXS Spectroscopy. *Inorg. Chem.* **57**, 7355–7361 (2018).

163. Ågren, H., Luo, Y., Gelmukhanov, F. & Jensen, H. J. Aa. Screening in resonant X-ray emission of molecules. *J. Electron Spectrosc. Relat. Phenom.* **82**, 125–134 (1996).

164. Cho, D., Rouxel, J. R., Mukamel, S., Kin-Lic Chan, G. & Li, Z. Stimulated X-ray Raman and Absorption Spectroscopy of Iron–Sulfur Dimers. *J. Phys. Chem. Lett.* **10**, 6664–6671 (2019).

165. Schweigert, I. V. & Mukamel, S. Probing valence electronic wave-packet dynamics by all x-ray stimulated Raman spectroscopy: A simulation study. *Phys. Rev. A* **76**, 012504 (2007).

166. Harbola, U. & Mukamel, S. Coherent stimulated x-ray Raman spectroscopy: Attosecond extension of resonant inelastic x-ray Raman scattering. *Phys. Rev. B* **79**, 085108 (2009).

167. Hua, W. *et al.* Monitoring conical intersections in the ring opening of furan by attosecond stimulated X-ray Raman spectroscopy. *Struct. Dyn.* **3**, 023601 (2016).

168. Weninger, C. Stimulated Electronic X-Ray Raman Scattering. *Phys. Rev. Lett.* **111**, (2013).

169. Weninger, C. & Rohringer, N. Stimulated resonant x-ray Raman scattering with incoherent radiation. *Phys. Rev. A* **88**, 053421 (2013).

170. Kimberg, V. & Rohringer, N. Stochastic stimulated electronic x-ray Raman spectroscopy. *Struct. Dyn.* **3**, 034101 (2016).

171. O'Neal, J. T. *et al.* Electronic Population Transfer via Impulsive Stimulated X-Ray Raman Scattering with Attosecond Soft-X-Ray Pulses. *Phys. Rev. Lett.* **125**, 073203 (2020).

172. Higley, D. J. *et al.* Stimulated resonant inelastic X-ray scattering in a solid. *Commun. Phys.* **5**, 1–12 (2022).

173. Arya, K. & Jha, S. S. Microscopic optical fields and mixing coefficients of x-ray and optical frequencies in solids. *Pramana* **2**, 116–125 (1974).

174. Pine, A. S. Self-Consistent-Field Theory of Linear and Nonlinear Crystalline Dielectrics Including Local-Field Effects. *Phys. Rev.* **139**, A901–A911 (1965).

175. Schweigert, I. V. & Mukamel, S. Coherent Ultrafast Core-Hole Correlation Spectroscopy: X-Ray Analogues of Multidimensional NMR. *Phys. Rev. Lett.* **99**, 163001 (2007).

176. Nazarkin, A., Podorov, S., Uschmann, I., Förster, E. & Sauerbrey, R. Nonlinear optics in the angstrom regime: Hard-x-ray frequency doubling in perfect crystals. *Phys. Rev. A* **67**, 041804 (2003).

177. Glover, T. E. *et al.* X-ray and optical wave mixing. *Nature* **488**, 603–608 (2012).

178. Tamasaku, K. & Ishikawa, T. Interference between Compton Scattering and X-Ray Parametric Down-Conversion. *Phys. Rev. Lett.* **98**, 244801 (2007).

179. Tamasaku, K., Sawada, K. & Ishikawa, T. Determining X-Ray Nonlinear Susceptibility of Diamond by the Optical Fano Effect. *Phys. Rev. Lett.* **103**, 254801 (2009).

180. Tamasaku, K., Sawada, K., Nishibori, E. & Ishikawa, T. Visualizing the local optical response to extreme-ultraviolet radiation with a resolution of λ/380. *Nat. Phys.* **7**, 705–708 (2011).

181. Schori, A. *et al.* Parametric Down-Conversion of X Rays into the Optical Regime. *Phys. Rev. Lett.* **119**, 253902 (2017).

182. Shwartz, S. *et al.* X-Ray Second Harmonic Generation. *Phys. Rev. Lett.* **112**, 163901 (2014).

183. Lam, R. K. *et al.* Soft X-Ray Second Harmonic Generation as an Interfacial Probe. *Phys. Rev. Lett.* **120**, 023901 (2018).

184. Yamamoto, Sh. *et al.* Element Selectivity in Second-Harmonic Generation of ${\mathrm{GaFeO}}_{3}$ by a Soft-X-Ray Free-Electron Laser. *Phys. Rev. Lett.* **120**, 223902 (2018).

185. Berger, E. *et al.* Extreme Ultraviolet Second Harmonic Generation Spectroscopy in a Polar Metal. *Nano Lett.* **21**, 6095–6101 (2021).

186. Schwartz, C. P. *et al.* Angstrom-Resolved Interfacial Structure in Buried Organic-Inorganic Junctions. *Phys. Rev. Lett.* **127**, 096801 (2021).

187. Sistrunk, E. *et al.* Extreme Ultraviolet Transient Grating Measurement of Insulator-Metal Transition Dynamics of VO2. in *19th International Conference on Ultrafast Phenomena* 09.Wed.P3.44 (OSA, 2014). doi:10.1364/UP.2014.09.Wed.P3.44.

188. Gaynor, J. D. *et al.* Solid state core-exciton dynamics in NaCl observed by tabletop attosecond four-wave mixing spectroscopy. *Phys. Rev. B* **103**, 245140 (2021).

189. Rottke, H. *et al.* Probing electron and hole colocalization by resonant four-wave mixing spectroscopy in the extreme ultraviolet. *Sci. Adv.* **8**, eabn5127 (2022).

190. Sander, M. *et al.* Spatiotemporal Coherent Control of Thermal Excitations in Solids. *Phys. Rev. Lett.* **119**, 075901 (2017).

191. Pudell, J.-E. *et al.* Full Spatiotemporal Control of Laser-Excited Periodic Surface Deformations. *Phys. Rev. Appl.* **12**, 024036 (2019).

192. Frazer, T. D. *et al.* Optical transient grating pumped X-ray diffraction microscopy for studying mesoscale structural dynamics. *Sci. Rep.* **11**, 19322 (2021).

193. Bencivenga, F. *et al.* Four-wave mixing experiments with extreme ultraviolet transient gratings. *Nature* **520**, 205–208 (2015).

194. Foglia, L. *et al.* First Evidence of Purely Extreme-Ultraviolet Four-Wave Mixing. *Phys. Rev. Lett.* **120**, 263901 (2018).

195. Bencivenga, F. *et al.* Nanoscale transient gratings excited and probed by extreme ultraviolet femtosecond pulses. *Sci. Adv.* **5**, eaaw5805 (2019).

196. Maznev, A. A. *et al.* Generation of coherent phonons by coherent extreme ultraviolet radiation in a transient grating experiment. *Appl. Phys. Lett.* **113**, 221905 (2018).

197. Maznev, A. A. *et al.* Generation and detection of 50 GHz surface acoustic waves by extreme ultraviolet pulses. *Appl. Phys. Lett.* **119**, 044102 (2021).

198. Bohinc, R. *et al.* Nonlinear XUV-optical transient grating spectroscopy at the Si L2,3–edge. *Appl. Phys. Lett.* **114**, 181101 (2019).

199. Naumenko, D. *et al.* Thermoelasticity of Nanoscale Silicon Carbide Membranes Excited by Extreme Ultraviolet Transient Gratings: Implications for Mechanical and Thermal Management. *ACS Appl. Nano Mater.* **2**, 5132–5139 (2019).

200. Ksenzov, D. *et al.* Nanoscale Transient Magnetization Gratings Created and Probed by Femtosecond Extreme Ultraviolet Pulses. *Nano Lett.* **21**, 2905–2911 (2021).

201. Yao, K. *et al.* All-Optical Switching on the Nanometer Scale Excited and Probed with Femtosecond Extreme Ultraviolet Pulses. *Nano Lett.* **22**, 4452–4458 (2022).

202. Rouxel, J. R. *et al.* Hard X-ray transient grating spectroscopy on bismuth germanate. *Nat. Photonics* **15**, 499–503 (2021).

203. Svetina, C. *et al.* Towards X-ray transient grating spectroscopy. *Opt. Lett.* **44**, 574–577 (2019).

204. Chen, Z., Gao, Y., Minch, B. C. & DeCamp, M. F. Coherent optical phonon generation in $Bi_3Ge_4O_{12}$. *J. Phys. Condens. Matter* **23**, 385402 (2011).

205. Peters, W. *et al.* Hard X-ray–Optical Transient Grating. in *2021 Conference on Lasers and Electro-Optics (CLEO)* 1–2 (2021).

206. Shi, H. & Zhu, D. Multi-Axis Nanopositioning System for the Hard X-ray Split-Delay System at the LCLS. *Synchrotron Radiat. News* **31**, 15–20 (2018).

207. Ukleev, V. *et al.* Effect of intense x-ray free-electron laser transient gratings on the magnetic domain structure of Tm:YIG. *J. Appl. Phys.* **133**, 123902 (2023).

208. Keefer, D., Cavaletto, S. M. & Rouxel, J. R. *Annual Review of Physical Chemistry*.

209. Roemelt, M., Maganas, D., DeBeer, S. & Neese, F. A combined DFT and restricted open-shell configuration interaction method including spin-orbit coupling: Application to transition metal L-edge X-ray absorption spectroscopy. *J. Chem. Phys.* **138**, 204101 (2013).

210. Norman, P. & Dreuw, A. Simulating X-ray Spectroscopies and Calculating Core-Excited States of Molecules. *Chem. Rev.* **118**, 7208–7248 (2018).

211. Vidal, M. L., Feng, X., Epifanovsky, E., Krylov, A. I. & Coriani, S. New and Efficient Equation-of-Motion Coupled-Cluster Framework for Core-Excited and Core-Ionized States. *J. Chem. Theory Comput.* **15**, 3117–3133 (2019).

212. Montorsi, F., Segatta, F., Nenov, A., Mukamel, S. & Garavelli, M. Soft X-ray Spectroscopy Simulations with Multiconfigurational Wave Function Theory: Spectrum Completeness, Sub-eV Accuracy, and Quantitative Reproduction of Line Shapes. *J. Chem. Theory Comput.* **18**, 1003–1016 (2022).

213. Tully, J. C. Molecular dynamics with electronic transitions. *J. Chem. Phys.* **93**, 1061–1071 (1990).

214. Meyer, H.-D., Manthe, U. & Cederbaum, L. S. The multi-configurational time-dependent Hartree approach. *Chem. Phys. Lett.* **165**, 73–78 (1990).

215. Ben-Nun, M. & Martinez, T. J. Ab initio quantum molecular dynamics. *Adv. Chem. Phys. Vol. 121* **121**, 439–512 (2002).

216. Makhov, D. V., Glover, W. J., Martinez, T. J. & Shalashilin, D. V. Ab initio multiple cloning algorithm for quantum nonadiabatic molecular dynamics. *J. Chem. Phys.* **141**, 054110 (2014).

217. Richter, M., Marquetand, P., González-Vázquez, J., Sola, I. & González, L. SHARC: ab Initio Molecular Dynamics with Surface Hopping in the Adiabatic Representation Including Arbitrary Couplings. *J. Chem. Theory Comput.* **7**, 1253–1258 (2011).

218. Reiter, S., Keefer, D. & de Vivie-Riedle, R. Exact Quantum Dynamics (Wave Packets) in Reduced Dimensionality. in *Quantum Chemistry and Dynamics of Excited States* 355–381 (John Wiley & Sons, Ltd, 2020). doi:10.1002/9781119417774.ch11.

219. Helmich-Paris, B. Simulating X-ray absorption spectra with complete active space self-consistent field linear response methods. *Int. J. Quantum Chem.* **121**, e26559 (2021).

220. Restricted active space configuration interaction methods for strong correlation: Recent developments - Casanova - 2022 - WIREs Computational Molecular Science - Wiley Online Library. https://wires.onlinelibrary.wiley.com/doi/abs/10.1002/wcms.1561?casa_token=8iUFrHrK1x4AAAAA:6c6665KroRLp7Z4-kv-U1-VBw-VPKfxY-zRbwih3Itr6payV7aR3hBPuxw5T8Mr14uUZPIpGh_CkLGsB.

221. Autschbach, J., Ziegler, T., van Gisbergen, S. J. A. & Baerends, E. J. Chiroptical properties from time-dependent density functional theory. I. Circular dichroism spectra of organic molecules. *J. Chem. Phys.* **116**, 6930–6940 (2002).

222. Lopata, K., Van Kuiken, B. E., Khalil, M. & Govind, N. Linear-Response and Real-Time Time-Dependent Density Functional Theory Studies of Core-Level Near-Edge X-Ray Absorption. *J. Chem. Theory Comput.* **8**, 3284–3292 (2012).

223. Andersen, J. H., Nanda, K. D., Krylov, A. I. & Coriani, S. Probing Molecular Chirality of Ground and Electronically Excited States in the UV–vis and X-ray Regimes: An EOM-CCSD Study. *J. Chem. Theory Comput.* **18**, 1748–1764 (2022).

224. Nanda, K. D. & Krylov, A. I. Cherry-picking resolvents: A general strategy for convergent coupled-cluster damped response calculations of core-level spectra. *J. Chem. Phys.* **153**, 141104 (2020).

225. Freund, I. Nonlinear X-ray diffraction. Determination of valence electron charge distributions. *Chem. Phys. Lett.* **12**, 583–588 (1972).

226. Shwartz, E. & Shwartz, S. Difference-frequency generation of optical radiation from two-color x-ray pulses. *Opt. Express* **23**, 7471–7480 (2015).

227. Rohringer, N. & Santra, R. X-ray nonlinear optical processes using a self-amplified spontaneous emission free-electron laser. *Phys. Rev. A* **76**, 033416 (2007).

228. Santra, R., Kryzhevoi, N. V. & Cederbaum, L. S. X-Ray Two-Photon Photoelectron Spectroscopy: A Theoretical Study of Inner-Shell Spectra of the Organic Para-Aminophenol Molecule. *Phys. Rev. Lett.* **103**, 013002 (2009).

229. Motomura, K. *et al.* Sequential multiphoton multiple ionization of atomic argon and xenon irradiated by X-ray free-electron laser pulses from SACLA. *J. Phys. B-At. Mol. Opt. Phys.* **46**, (2013).

230. Mazza, T. *et al.* Sensitivity of nonlinear photoionization to resonance substructure in collective excitation. *Nat. Commun.* **6**, 6799 (2015).

231. Popova-Gorelova, D., Guskov, V. & Santra, R. Microscopic electron dynamics in nonlinear optical response of solids. Preprint at https://doi.org/10.48550/arXiv.2009.07527 (2020).

232. Popova-Gorelova, D. & Santra, R. Atomic-scale imaging of laser-driven electron dynamics in solids using subcycle-resolved x-ray-optical wave mixing. Preprint at https://doi.org/10.48550/arXiv.2012.10334 (2020).

233. Keefer, D. *et al.* Monitoring molecular vibronic coherences in a bichromophoric molecule by ultrafast X-ray spectroscopy. *Chem. Sci.* **12**, 5286–5294 (2021).

234. Bennett, K., Kowalewski, M., Rouxel, J. R. & Mukamel, S. Monitoring molecular nonadiabatic dynamics with femtosecond X-ray diffraction. *Proc. Natl. Acad. Sci.* **115**, 6538–6547 (2018).

235. Shakya, Y., Inhester, L., Arnold, C., Welsch, R. & Santra, R. Ultrafast time-resolved x-ray absorption spectroscopy of ionized urea and its dimer through ab initio nonadiabatic dynamics. *Struct. Dyn.* **8**, 034102 (2021).

236. H. List, N., L. Dempwolff, A., Dreuw, A., Norman, P. & J. Martínez, T. Probing competing relaxation pathways in malonaldehyde with transient X-ray absorption spectroscopy. *Chem. Sci.* **11**, 4180–4193 (2020).

237. Keefer, D., Schnappinger, T., de Vivie-Riedle, R. & Mukamel, S. Visualizing conical intersection passages via vibronic coherence maps generated by stimulated ultrafast X-ray Raman signals. *Proc. Natl. Acad. Sci.* **117**, 24069–24075 (2020).

238. Nenov, A., Segatta, F., Bruner, A., Mukamel, S. & Garavelli, M. X-ray linear and non-linear spectroscopy of the ESCA molecule. *J. Chem. Phys.* **151**, 114110 (2019).

239. Kowalewski, M. Catching Conical Intersections in the Act: Monitoring Transient Electronic Coherences by Attosecond Stimulated X-Ray Raman Signals. *Phys. Rev. Lett.* **115**, (2015).

240. Rouxel, J. R., Kowalewski, M., Bennett, K. & Mukamel, S. X-Ray Sum Frequency Diffraction for Direct Imaging of Ultrafast Electron Dynamics. *Phys. Rev. Lett.* **120**, 243902 (2018).

241. Neville, S. P., Chergui, M., Stolow, A. & Schuurman, M. S. Ultrafast X-Ray Spectroscopy of Conical Intersections. *Phys. Rev. Lett.* **120**, (2018).

242. Keefer, D. *et al.* Imaging conical intersection dynamics during azobenzene photoisomerization by ultrafast X-ray diffraction. *Proc. Natl. Acad. Sci.* **118**, e2022037118 (2021).

243. Amann, J. *et al.* Demonstration of self-seeding in a hard-X-ray free-electron laser. *Nat. Photonics* **6**, 693–698 (2012).

244. LCLS-II. *Linac Coherent Light Source* https://lcls.slac.stanford.edu/lcls-ii (2017).

245. Cavaletto, S. M., Keefer, D. & Mukamel, S. High Temporal and Spectral Resolution of Stimulated X-Ray Raman Signals with Stochastic Free-Electron-Laser Pulses. *Phys. Rev. X* **11**, 011029 (2021).

246. Biggs, J. D., Zhang, Y., Healion, D. & Mukamel, S. Watching energy transfer in metalloporphyrin heterodimers using stimulated X-ray Raman spectroscopy. *Proc. Natl. Acad. Sci.* **110**, 15597–15601 (2013).

247. Kimberg, V. *et al.* Stimulated X-ray Raman scattering – a critical assessment of the building block of nonlinear X-ray spectroscopy. *Faraday Discuss.* **194**, 305–324 (2016).

248. Gschwendtner, E. & Muggli, P. Plasma wakefield accelerators. *Nat. Rev. Phys.* **1**, 246–248 (2019).

249. Wang, W. *et al.* Free-electron lasing at 27 nanometres based on a laser wakefield accelerator. *Nature* **595**, 516–520 (2021).

250. Galletti, M. *et al.* Stable Operation of a Free-Electron Laser Driven by a Plasma Accelerator. *Phys. Rev. Lett.* **129**, 234801 (2022).

251. Labat, M. *et al.* Seeded free-electron laser driven by a compact laser plasma accelerator. *Nat. Photonics* **17**, 150–156 (2023).

252. Trebino, R. *Frequency-Resolved Optical Gating: The Measurement of Ultrashort Laser Pulses: The Measurement of Ultrashort Laser Pulses*. (Springer Science & Business Media, 2000).

253. Peters, W. K. *et al.* All-optical single-shot complete electric field measurement of extreme ultraviolet free electron laser pulses. *Optica* **8**, 545–550 (2021).

254. Gauthier, D. *et al.* Spectrotemporal Shaping of Seeded Free-Electron Laser Pulses. *Phys. Rev. Lett.* **115**, 114801 (2015).

255. Prince, K. C. *et al.* Coherent control with a short-wavelength free-electron laser. *Nat. Photonics* **10**, 176–179 (2016).

256. Cavaletto, S. M. *et al.* Unveiling the spatial distribution of molecular coherences at conical intersections by covariance X-ray diffraction signals. *Proc. Natl. Acad. Sci.* **118**, e2105046118 (2021).

257. Ratner, D., Cryan, J. P., Lane, T. J., Li, S. & Stupakov, G. Pump-Probe Ghost Imaging with SASE FELs. *Phys. Rev. X* **9**, 011045 (2019).

258. Kayser, Y. *et al.* Core-level nonlinear spectroscopy triggered by stochastic X-ray pulses. *Nat. Commun.* **10**, 4761 (2019).

259. Driver, T. *et al.* Attosecond transient absorption spooktroscopy: a ghost imaging approach to ultrafast absorption spectroscopy. *Phys. Chem. Chem. Phys.* **22**, 2704–2712 (2020).

260. Gorobtsov, O. Y. *et al.* Seeded X-ray free-electron laser generating radiation with laser statistical properties. *Nat. Commun.* **9**, 4498 (2018).

261. Li, K. *et al.* Ghost-imaging-enhanced noninvasive spectral characterization of stochastic x-ray free-electron-laser pulses. *Commun. Phys.* **5**, 1–8 (2022).

262. Kalz, K. F. *et al.* Future Challenges in Heterogeneous Catalysis: Understanding Catalysts under Dynamic Reaction Conditions. *Chemcatchem* **9**, 17–29 (2017).

263. Yang, Y. *et al.* Operando Methods in Electrocatalysis. *ACS Catal.* **11**, 1136–1178 (2021).

264. Singh, J., Lamberti, C. & Bokhoven, J. A. van. Advanced X-ray absorption and emission spectroscopy : in situ catalytic studies. *Chem. Soc. Rev.* **39**, 4754–4766 (2010).

265. Beye, M. *et al.* Non-linear soft x-ray methods on solids with MUSIX—the multi-dimensional spectroscopy and inelastic x-ray scattering endstation. *J. Phys. Condens. Matter* **31**, 014003 (2018).

266. Chakraborti, P. *et al.* Higher-Order X-ray - Optical Wave Mixing. *SPring-8SACLA利用研究成果集* **10**, 409–412 (2022).

267. Alagna, L. *et al.* X-Ray Natural Circular Dichroism. *Phys. Rev. Lett.* **80**, 4799–4802 (1998).

268. Peacock, R. D. & Stewart, B. Natural Circular Dichroism in X-ray Spectroscopy. *J. Phys. Chem. B* **105**, 351–360 (2001).

269. Turchini, S. *et al.* Core Electron Transitions as a Probe for Molecular Chirality: Natural Circular Dichroism at the Carbon K-edge of Methyloxirane. *J. Am. Chem. Soc.* **126**, 4532–4533 (2004).

270. Tanaka, M., Nakagawa, K., Agui, A., Fujii, K. & Yokoya, A. First observation of natural circular dichroism for biomolecules in soft x-ray region studied with a polarizing undulator. *Phys. Scr.* **2005**, 873 (2005).

271. Rouxel, J. R. *et al.* Hard X-ray helical dichroism of disordered molecular media. *Nat. Photonics* **16**, 570–574 (2022).

272. Mincigrucci, R. *et al.* Element- and enantiomer-selective visualization of molecular motion in real-time. *Nat. Commun.* **14**, 386 (2023).

273. Byers, J. D., Yee, H. I., Petralli-Mallow, T. & Hicks, J. M. Second-harmonic generation circular-dichroism spectroscopy from chiral monolayers. *Phys. Rev. B* **49**, 14643–14647 (1994).

274. Petralli-Mallow, T., Wong, T. M., Byers, J. D., Yee, H. I. & Hicks, J. M. Circular dichroism spectroscopy at interfaces: a surface second harmonic generation study. *J. Phys. Chem.* **97**, 1383–1388 (1993).

275. Kauranen, M., Verbiest, T., Maki, J. J. & Persoons, A. Second-harmonic generation from chiral surfaces. *J. Chem. Phys.* **101**, 8193–8199 (1994).

276. Verbiest, T., Kauranen, M., Van Rompaey, Y. & Persoons, A. Optical Activity of Anisotropic Achiral Surfaces. *Phys. Rev. Lett.* **77**, 1456–1459 (1996).

277. Verbiest, T., Kauranen, M. & Persoons, A. Second-order nonlinear optical properties of chiral thin films. *J. Mater. Chem.* **9**, 2005–2012 (1999).

278. Belkin, M. A., Han, S. H., Wei, X. & Shen, Y. R. Sum-Frequency Generation in Chiral Liquids near Electronic Resonance. *Phys. Rev. Lett.* **87**, 113001 (2001).

279. Belkin, M. A., Shen, Y. R. & Flytzanis, C. Coupled-oscillator model for nonlinear optical activity. *Chem. Phys. Lett.* **363**, 479–485 (2002).

280. Belkin†, M. A. & Shen‡, Y. R. Non-linear optical spectroscopy as a novel probe for molecular chirality. *Int. Rev. Phys. Chem.* **24**, 257–299 (2005).

281. Fischer, P., Beckwitt, K., Wise, F. W. & Albrecht, A. C. The chiral specificity of sum-frequency generation in solutions. *Chem. Phys. Lett.* **352**, 463–468 (2002).

282. Lee, T., Rhee, H. & Cho, M. Femtosecond Vibrational Sum-Frequency Generation Spectroscopy of Chiral Molecules in Isotropic Liquid. *J. Phys. Chem. Lett.* **9**, 6723–6730 (2018).

283. Song, Z., Zhang, T., Fang, Z. & Fang, C. Quantitative mappings between symmetry and topology in solids. *Nat. Commun.* **9**, 3530 (2018).

284. Gatti, G. *et al.* Radial Spin Texture of the Weyl Fermions in Chiral Tellurium. *Phys. Rev. Lett.* **125**, 216402 (2020).

285. Cochran, T. A. *et al.* Visualizing Higher-Fold Topology in Chiral Crystals. *Phys. Rev. Lett.* **130**, 066402 (2023).

286. TERAZIMA, M. A transient grating detection method of circular dichroism. *Mol. Phys.* **88**, 1223–1236 (1996).

287. R. Rouxel, J., Zhang, Y. & Mukamel, S. X-ray Raman optical activity of chiral molecules. *Chem. Sci.* **10**, 898–908 (2019).

288. Rouxel, J. R., Kowalewski, M. & Mukamel, S. Photoinduced molecular chirality probed by ultrafast resonant X-ray spectroscopy. *Struct. Dyn.* **4**, 044006 (2017).

289. Bencivenga, F. *et al.* Four-wave-mixing experiments with seeded free electron lasers. *Faraday Discuss.* **194**, 283–303 (2016).

290. Rouxel, J. R. & Mukamel, S. Molecular Chirality and Its Monitoring by Ultrafast X-ray Pulses. *Chem. Rev.* **122**, 16802–16838 (2022).

291. Rouxel, J. R., Rajabi, A. & Mukamel, S. Chiral Four-Wave Mixing Signals with Circularly Polarized X-ray Pulses. *J. Chem. Theory Comput.* **16**, 5784–5791 (2020).

292. Schenkl, S. *et al.* Insights into excited-state and isomerization dynamics of bacteriorhodopsin from ultrafast transient UV absorption. *Proc. Natl. Acad. Sci.* **103**, 4101–4106 (2006).

293. Polli, D. *et al.* Conical intersection dynamics of the primary photoisomerization event in vision. *Nature* **467**, 440–443 (2010).

294. Schreier, W. J., Gilch, P. & Zinth, W. Early Events of DNA Photodamage. *Annu. Rev. Phys. Chem.* **66**, 497–519 (2015).

295. Ebadi, H. Tracking of Azobenzene Isomerization by X-ray Emission Spectroscopy. *J. Phys. Chem. A* **118**, 7832–7837 (2014).

296. Hua, W., Mukamel, S. & Luo, Y. Transient X-ray Absorption Spectral Fingerprints of the S1 Dark State in Uracil. *J. Phys. Chem. Lett.* **10**, 7172–7178 (2019).

297. Nam, Y. *et al.* Time-Resolved Optical Pump-Resonant X-ray Probe Spectroscopy of 4-Thiouracil: A Simulation Study. *J. Chem. Theory Comput.* **18**, 3075–3088 (2022).

298. Segatta, F. *et al.* Exploring the capabilities of optical pump X-ray probe NEXAFS spectroscopy to track photo-induced dynamics mediated by conical intersections. *Faraday Discuss.* **221**, 245–264 (2020).

299. Chang, K. F. *et al.* Revealing electronic state-switching at conical intersections in alkyl iodides by ultrafast XUV transient absorption spectroscopy. *Nat. Commun.* **11**, 4042 (2020).

300. Timmers, H. *et al.* Disentangling conical intersection and coherent molecular dynamics in methyl bromide with attosecond transient absorption spectroscopy. *Nat. Commun.* **10**, 3133 (2019).

301. Nam, Y. *et al.* Conical Intersection Passages of Molecules Probed by X-ray Diffraction and Stimulated Raman Spectroscopy. *J. Phys. Chem. Lett.* **12**, 12300–12309 (2021).

302. M. Freixas, V., Keefer, D., Tretiak, S., Fernandez-Alberti, S. & Mukamel, S. Ultrafast coherent photoexcited dynamics in a trimeric dendrimer probed by X-ray stimulated-Raman signals. *Chem. Sci.* **13**, 6373–6384 (2022).

303. Polishchuk, S. *et al.* Nanoscale-Resolved Surface-to-Bulk Electron Transport in CsPbBr3 Perovskite. *Nano Lett.* **22**, 1067–1074 (2022).

304. Consani, C., Bram, O., van Mourik, F., Cannizzo, A. & Chergui, M. Energy transfer and relaxation mechanisms in Cytochrome c. *Chem. Phys.* **396**, 108–115 (2012).

305. Chenu, A. & Scholes, G. D. Coherence in Energy Transfer and Photosynthesis. *Annu. Rev. Phys. Chem. Vol 66* **66**, 69–96 (2015).

306. Bacellar, C. & et al. Ultrafast Energy Transfer from photoexcited Tryptophan to the Haem in Cytochrome c. *Journal of Physical Chemistry Letters* (2023).

307. Zeiger, H. J. *et al.* Theory for displacive excitation of coherent phonons. *Phys. Rev. B* **45**, 768–778 (1992).

308. Mukamel, S., Healion, D., Zhang, Y. & Biggs, J. D. Multidimensional attosecond resonant X-ray spectroscopy of molecules: Lessons from the optical regime. *Annu. Rev. Phys. Chem.* **64**, 101–127 (2013).

309. Al-Haddad, A. *et al.* Observation of site-selective chemical bond changes via ultrafast chemical shifts. *Nat. Commun.* **13**, 7170 (2022).

310. El Nahhas, A. *et al.* X-ray Absorption Spectroscopy of Ground and Excited Rhenium-Carbonyl Diimine-Complexes: Evidence for a Two-Center Electron Transfer. *J. Phys. Chem. A* **117**, 361–369 (2013).

311. 1: Coherent Spectroscopy and the Nonlinear Polarization. *Chemistry LibreTexts* https://chem.libretexts.org/Bookshelves/Physical_and_Theoretical_Chemistry_Textbook_Maps/Book%3A_Nonlinear_and_Two-Dimensional_Spectroscopy_(Tokmakoff)/01%3A_Coherent_Spectroscopy_and_the_Nonlinear_Polarization (2021).

312. Johnson, J. A. *et al.* Direct Measurement of Room-Temperature Nondiffusive Thermal Transport Over Micron Distances in a Silicon Membrane. *Phys. Rev. Lett.* **110**, 025901 (2013).

313. Bencivenga, F. & Masciovecchio, C. FEL-based transient grating spectroscopy to investigate nanoscale dynamics. *Nucl. Instrum. Methods Phys. Res. Sect. Accel. Spectrometers Detect. Assoc. Equip.* **606**, 785–789 (2009).